Draft version June 11, 2025
Typeset using LaTeX **twocolumn** style in AASTeX631

JWST/NIRSpec Observations of High Ionization Emission Lines in Galaxies at High Redshift

Mengtao Tang [1], Daniel P. Stark,[2] Adèle Plat,[3] Anna Feltre,[4] Harley Katz,[5] Peter Senchyna,[6] Charlotte A. Mason,[7,8] Lily Whitler,[1] Zuyi Chen,[1] and Michael W. Topping[1]

[1] *Steward Observatory, University of Arizona, 933 N Cherry Ave, Tucson, AZ 85721, USA*
[2] *Department of Astronomy, University of California, Berkeley, Berkeley, CA 94720, USA*
[3] *Institute for Physics, Laboratory for Galaxy Evolution and Spectral Modelling, Ecole Polytechnique Federale de Lausanne, Observatoire de Sauverny, Chemin Pegasi 51, CH-1290 Versoix, Switzerland*
[4] *INAF - Osservatorio Astrofisico di Arcetri, Largo E. Fermi 5, I-50125, Firenze, Italy*
[5] *Department of Astronomy & Astrophysics, University of Chicago, 5640 S Ellis Avenue, Chicago, IL 60637, USA*
[6] *The Observatories of the Carnegie Institution for Science, 813 Santa Barbara Street, Pasadena, CA 91101, USA*
[7] *Cosmic Dawn Center (DAWN)*
[8] *Niels Bohr Institute, University of Copenhagen, Jagtvej 128, 2200 Copenhagen N, Denmark*

ABSTRACT

JWST spectroscopy has built large emission line samples at $z \gtrsim 4$, but it has yet to confidently reveal many galaxies with the hard radiation fields commonly associated with AGN photoionization. While this may indicate a weaker UV ionizing spectrum in many $z > 4$ AGNs or obscuration from dense neutral gas and dust, the complete picture remains unclear owing to the small number of deep rest-UV spectra. Here we characterize the strength of high ionization lines in 53 new galaxies observed with NIRSpec $R = 2700$ grating spectroscopy. We present new detections of narrow N V λ1240 in two galaxies. One is a previously-confirmed $z = 6.98$ Little Red Dot (LRD) with broad Hβ, and the other is a $z = 8.72$ galaxy with a narrow line spectrum. Neither source exhibits C IV or He II emission, indicating large N V/C IV and N V/He II ratios that may reflect a combination of nitrogen-enhancement and resonant scattering effects. We investigate the incidence of narrow high ionization lines in a large database of 851 NIRSpec grating spectra, and we separately quantify the fraction of LRDs with narrow high ionization UV emission lines. Our results likely suggest that hard radiation fields are indeed present in a small subset of LRDs ($12.5^{+23.7}_{-10.4}$%) and UV-selected galaxies ($2.2^{+1.7}_{-1.0}$%) at $z > 4$. The identification of narrow high ionization lines in the population of LRDs with strong Balmer absorption suggests the dense neutral hydrogen gas may not uniformly cover the nucleus. The N V/C IV and N V/He II ratios suggest that efforts to identify high ionization lines should extend down in wavelength to the N V doublet.

Keywords: High-redshift galaxies (734); Active galactic nuclei (16)

1. INTRODUCTION

One decade ago, the first rest-frame ultraviolet (UV) metal emission lines (C III], C IV) were detected in bright $z \simeq 6-7$ galaxies (Stark et al. 2015a,b, 2017; Laporte et al. 2017; Mainali et al. 2017; Hutchison et al. 2019; Topping et al. 2021). The equivalent widths (EWs) were found to be over an order of magnitude greater than what is common at $z \simeq 2-3$, suggesting that there might be significant evolution in the gas conditions and radiation field at $z \gtrsim 6$. The origin of the hard radiation field was not clear with ground-based data, with some arguing that an active galactic nucleus (AGN) was responsible (Nakajima et al. 2018) and others suggesting the presence of low metallicity massive stars (e.g., Mainali et al. 2017; Stark et al. 2017). Regardless of the powering mechanism, the discovery of such strong emission (EW $> 20-40$ Å) led to the suggestion that the UV metal lines would be readily detectable in galaxies at $z \simeq 10-15$ with NIRSpec (Jakobsen et al. 2022; Böker et al. 2023) spectroscopy, providing a viable path toward characterizing the stars, gas and ionizing sources in the most distant galaxies that *JWST* (Gardner et al. 2023; Rigby et al. 2023) discovers.

tangmtasua@arizona.edu

This prediction has been borne out with *JWST* rest-frame UV spectroscopy. In the last year, we have seen the redshift frontier extended to $z \simeq 14$ (Carniani et al. 2024), with UV metal lines often providing our best path toward characterization of the most distant galaxies that have been discovered (Bunker et al. 2023; Carniani et al. 2024; Castellano et al. 2024; D'Eugenio et al. 2024; Hsiao et al. 2024; Napolitano et al. 2025). Deeper spectroscopy has been obtained of several of the brightest $z \gtrsim 6$ galaxies showing intense C III] and C IV emission (Topping et al. 2024a, 2025a). These spectra show a suite of intense lines from species with ionization energies up to 54 eV (the He^+ edge), but yet higher ionization lines are not seen (i.e. N V, [Ne IV], [Ne V]). The implied radiation field appears consistent with stellar photoionization. While it is plausible that AGN contribute significantly to these lines, there is no clear indication from the observed extreme UV (EUV) line ratios.

If the majority of galaxies with strong UV metal lines at $z \gtrsim 6$ are (mostly) dominated by stars, the question remains whether a separate population of AGNs with high ionization line emission is also present. While large samples of $z \gtrsim 4$ broad-line (Type I) AGNs (BL AGNs) have been revealed with *JWST* spectroscopy (e.g., Kocevski et al. 2023; Kokorev et al. 2023; Übler et al. 2023; Furtak et al. 2024; Greene et al. 2024; Kocevski et al. 2024; Maiolino et al. 2024a; Matthee et al. 2024; Übler et al. 2024), there have been relatively few robust detections of very high ionization lines (e.g., Brinchmann 2023; Scholtz et al. 2023; Chisholm et al. 2024; Mazzolari et al. 2024a; Silcock et al. 2024; Treiber et al. 2024) commonly seen in narrow line (Type II) AGN (NL AGN) spectra. Additionally the rest-frame UV spectra of the BL AGN discovered with *JWST* have thus far not revealed broad permitted high ionization line emission in the rest-frame UV. It has been suggested that the absence of high ionization lines in the Type I AGN may be a consequence of super-Eddington accretion, with photon trapping in the thick accretion disk leading to an intrinsically weaker UV spectrum (e.g., Pognan et al. 2020; Lambrides et al. 2024). Additionally, if the BL AGN are surrounded by extremely dense neutral gas with a near-unity covering fraction and the $n = 2$ level of hydrogen populated (e.g., de Graaff et al. 2025; Inayoshi & Maiolino 2025; Ji et al. 2025; Naidu et al. 2025), the emergent UV lines would face significant opacity, and the ionizing continuum would be attenuated before reaching the narrow line emitting region. Both factors may contribute to the absence of high ionization line emission.

Progress in characterizing the UV radiation field of $z \gtrsim 4$ AGNs will only be possible with larger samples of deep rest-frame UV spectra. Toward this end, we present a search for high ionization line emission in 851 $z \gtrsim 4$ galaxies with NIRSpec grating spectra ($R = 1000$ or $R = 2700$), including a sample of 18 $z \gtrsim 4$ galaxies confirmed as BL AGN with *JWST* spectroscopy. This database includes new observations from a NIRSpec program (GO 4287, PI: Mason) using the high resolution ($R = 2700$) G140H/F100LP grating to sample the rest-frame UV of $z \gtrsim 6$ galaxies in the Extended Groth Strip (EGS) field (Davis et al. 2007). These new observations have revealed two detections of narrow emission lines near the N V resonance. One is found in a BL AGN at $z = 6.98$ (CEERS-7902, Labbé et al. 2023; Kocevski et al. 2024), whereas the spectral energy distribution (SED) of the other is suggestive of a fairly typical star forming galaxy at $z = 8.72$ (CEERS-1025, Nakajima et al. 2023; Tang et al. 2023). In this paper, we use our full database to assess the fraction of $z \gtrsim 4$ galaxies showing high ionization lines, as might be expected from an AGN power law spectrum with significant UV continuum output. We also quantify the strength of high ionization line emission (narrow and broad) in $z \gtrsim 4$ Little Red Dots (LRDs; Matthee et al. 2024) that have been confirmed to show broad line hydrogen lines in the rest-frame optical. We present and describe new rest-frame UV spectra for two LRDs (CEERS-7902 and CEERS-10444).

The organization of this paper is as follows. In Section 2, we describe the GO 4287 observations and the data analysis. We then characterize the spectroscopic properties of the two likely N V emitters (CEERS-1025, CEERS-7902) and a LRD (CEERS-10444) from GO 4287 in Section 3. In Section 3.4, we compare the implied N V line ratios to expectations from photoionization models. We then search for high ionization line emission in the full archival JWST/NIRSpec sample at $z > 4$ in Section 4 and discuss implications of the census in Section 5. Finally, we summarize our conclusions in Section 6. Throughout the paper, we adopt a Λ-dominated, flat universe with $\Omega_\Lambda = 0.7$, $\Omega_M = 0.3$, and $H_0 = 70$ km s^{-1} Mpc^{-1}. All magnitudes are quoted in the AB system (Oke & Gunn 1983) and all EWs are quoted in the rest frame.

2. SPECTROSCOPIC DATA AND ANALYSIS

In this section, we describe the JWST/NIRSpec spectroscopic data obtained from the Cycle 2 program GO 4287 (PI: C. Mason). This program targets high redshift galaxies in the NIRCam (Rieke et al. 2005, 2023) imaging footprint of the EGS field. The spectra were obtained using JWST/NIRSpec in multi-object spectroscopy mode in 2024 March. We observed three micro-

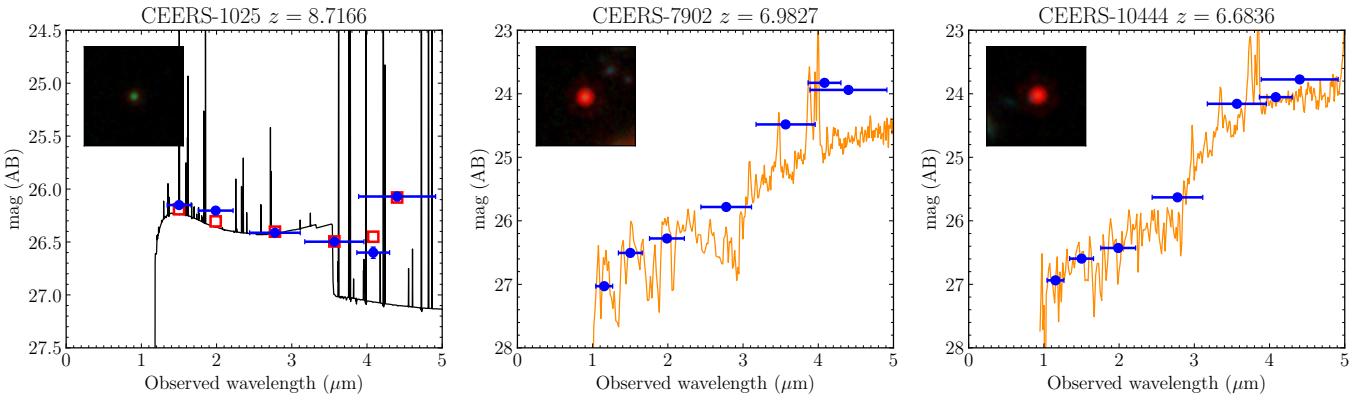

Figure 1. SEDs of the two N V emitters CEERS-1025 (left) and CEERS-7902 (LRD; middle), as well as CEERS-10444 (LRD; right). Observed photometry is shown by blue circles. Left: We show the `BEAGLE` model (Chevallard & Charlot 2016) spectrum of CEERS-1025 as the black line and the synthetic photometry as red squares. Middle and right: We show the NIRSpec prism spectra of CEERS-7902 and CEERS-10444 obtained from RUBIES (de Graaff et al. 2024) as the orange lines. We insert the postage stamp ($1.5'' \times 1.5''$) of each object. The RGB image are composed of images of F115W, F200W, and F444W bands.

shutter assembly (MSA; Ferruit et al. 2022) mask configurations. The primary targets placed on these configurations are galaxies in candidate overdensities that may trace ionized bubbles. We provide a brief summary of the observations here. A full description and catalog will be presented in Whitler et al. (2025, in prep).

The observations were conducted with MSA configurations using the high-resolution ($R = 2700$) grating/filter pair G140H/F100LP (targeting the rest-frame UV) and the medium-resolution ($R = 1000$) grating/filter pair G395M/F290LP (targeting the rest-frame optical). The total exposure time was 14005 s for G140H/F100LP and 3501 s for G395M/F290LP. For each slit on the MSA, we used a 3-shutter slitlet and observed with 3-nod pattern for dithering.

The 2D NIRSpec spectra were reduced following the procedures described in Topping et al. (2025a) using the standard JWST data reduction pipeline[1] (Bushouse et al. 2024). The 1D spectra are then extracted from the reduced 2D spectra using a boxcar extraction. The typical extraction aperture is 5 pixels (~ 0.5 arcsec in the spatial direction). For the G140H/F100LP spectra, we find that one resolution element corresponds to $\simeq 111$ km s^{-1}). In these spectra, the median 3σ limiting line flux is 3.5×10^{-19} erg s^{-1} cm^{-2} for an unresolved emission line (in the spectral direction) produced by a point source. At this limiting flux, we can detect weak emission lines (5 Å) in the rest-frame UV for moderately faint continuum sources ($H = 27.0$) at $z \simeq 8$. For G395M/F290LP spectra, the spectral resolution is closer to $\simeq 300$ km s^{-1} and the median 3σ limiting line flux is 4.6×10^{-19} erg s^{-1} cm^{-2}.

For this analysis, we have also updated our reductions of spectra of other targets in the EGS field, building on our earlier work (Tang et al. 2023; Chen et al. 2024; Tang et al. 2024). In particular, we add in new data from the Red Unknowns: Bright Infrared Extragalactic Survey (RUBIES, GO 4233, PIs: A. de Graaff & G. Brammer; de Graaff et al. 2024) program, reduced following the same procedures we used to process the GO 4287 data. The RUBIES observations target the EGS and the Ultra Deep Survey (UDS) fields with *JWST*/NIRSpec, using both the low resolution ($R \sim 100$) prism (covering $0.6 - 5.3$ μm) and medium resolution grating/filter pair G395M/F290LP (covering $2.8 - 5.2$ μm). We refer readers to de Graaff et al. (2024) for a detailed description.

In this paper, we present the spectra of two galaxies (CEERS-1025 and CEERS-7902) for which we have detected an emission line near the N V doublet. CEERS-1025 was first observed by the Cosmic Evolution Early Release Science[2] (CEERS, ERS 1345, PI: S. Finkelstein; Finkelstein et al. 2025) program, providing $R = 1000$ spectra targeting from the rest-frame UV to optical. To maximize the S/N, we generate a composite G395M spectrum for CEERS-1025 by stacking the GO 4287 and CEERS $R = 1000$ grating spectrum (Tang et al. 2023), with the weighting set by the exposure times. CEERS-7902 was also observed by RUBIES (and discussed in Wang et al. 2024a; Kocevski et al. 2024). We generate a composite G395M spectrum for CEERS-7902 by stacking the GO 4287 and RUBIES grating spectra. We also present new spectra of a third galaxy, CEERS-10444, a LRD that was also observed in the RUBIES program. We describe our new rest-frame UV spectrum and stack

[1] https://github.com/spacetelescope/jwst

[2] https://ceers.github.io/

our rest-frame optical G395M spectrum with that obtained in the RUBIES program. In the following analysis, we will use GO 4287 G140H spectra and the composite G395M spectra.

We perform the emission line measurements for CEERS-1025, CEERS-7902, and CEERS-10444 as follows. For emission lines detected with S/N $>$ 5, we measure the line fluxes, centroids, widths, and EWs of each galaxy by fitting the line profiles and nearby continua with Gaussian functions on top of linear functions. For isolated emission lines, we use a single Gaussian. For emission lines that are close in wavelength (i.e., Hγ and [O III] λ4363), we fit with multiple Gaussians simultaneously. In the case of emission lines with broad components, we fit the line with a narrow Gaussian on top of a broad Gaussian. For emission lines detected with lower S/N ($<$ 5), we calculate the line fluxes using direct integration. We note that Gaussian fit and direct integration result in similar line fluxes for emission lines with S/N $>$ 5. We evaluate the uncertainties of the line fluxes and EWs using the following procedure. We resample the flux densities of each spectrum 1000 times by taking the observed flux densities as the mean values and the errors as standard deviations. Then we compute the line fluxes and EWs from the resampled spectra of each galaxy using the same approach described above. We take the standard deviation of these measurements as the uncertainty. The same analysis is presented to the other 55 $z > 4$ galaxies in the GO 4287 spectra. While these will be presented in more detail in a later work (Whitler et al. 2025, in prep), we will compare the line ratios of the N V emitters to those in the full sample (in addition to other sources in the archive) to place the likely N V detections in context.

Table 1. Systemic redshifts and rest-frame UV to optical emission line fluxes ($\times 10^{-19}$ erg s^{-1} cm^{-2}) of the two N V emitters. We show 3σ upper limits for non-detections.

	CEERS-1025	CEERS-7902
$z_{\rm sys}$	8.7166	6.9827
N V λ1239	< 5.2	12.0 ± 1.5
N V λ1243	14.0 ± 2.3	< 3.2
[N IV] λ1483	< 4.7	< 2.5
N IV] λ1486	< 5.0	< 2.4
C IV λ1548	< 5.3	< 2.2
C IV λ1551	< 4.7	< 2.4
He II λ1640	< 5.3	< 2.5
O III] λ1661	< 5.6	< 2.2
O III] λ1666	< 5.0	< 2.4
N III] λ1746	< 5.9	-
N III] λ1748	< 5.6	-
[C III] λ1907	-	< 2.9
C III] λ1909	-	3.5 ± 1.2
[O II] λ3728	8.9 ± 2.1	2.8 ± 1.5
[Ne III] λ3869	3.0 ± 1.2	5.5 ± 1.3
Hγ (total)	6.9 ± 1.9	11.2 ± 3.0
Hγ (narrow)	-	4.0 ± 1.3^{a}
Hγ (broad)	-	7.2 ± 2.7^{b}
[O III] λ4363	3.6 ± 1.4	7.3 ± 1.4
Hβ (total)	14.5 ± 2.4	50.2 ± 3.9
Hβ (narrow)	-	5.9 ± 1.1^{a}
Hβ (broad)	-	44.4 ± 3.7^{b}
[O III] λ4959	21.9 ± 2.3	19.0 ± 1.3
[O III] λ5007	63.5 ± 2.8	57.7 ± 1.7
He I λ5877	-	5.7 ± 2.1
[O I] λ6302	-	4.4 ± 1.1

NOTE—a: Narrow component of the Hγ or Hβ emission line of CEERS-7902. b: Broad component of the Hγ or Hβ of CEERS-7902.

3. HIGH IONIZATION EMISSION IN GO 4287

We present new NIRSpec observations of CEERS-1025 (Section 3.1), CEERS-7902 (Section 3.2), and CEERS-10444 (Section 3.3) from GO 4287. We first discuss what was known about both galaxies from earlier *JWST* observations before describing the new emission line detections. Then we discuss the interpretation of line ratios between N V and other UV lines in Section 3.4.

3.1. *Spectroscopy of $z = 8.72$ galaxy CEERS-1025*

CEERS-1025 (R.A. = 214.967594, Decl. = +52.933005) is a bright galaxy ($m_{\rm F150W}$ = 26.2, $M_{\rm UV}$ = -21.2) at z = 8.72. The redshift of this object was first confirmed from the CEERS observations using the medium-resolution NIRSpec grating (G140M/F100LP, G235M/F170LP, G395M/F290LP) (e.g., Nakajima et al. 2023; Tang et al. 2023). These observations cover rest-frame wavelengths of 1010$-$1120 Å and 1245$-$5350 Å, with a chip gap leading to the missing spectral coverage between Lyα and N V emission.

As described in Tang et al. (2023), the NIRCam SED from CEERS (left panel of Figure 1) reveals a blue UV slope ($\beta = -2.5$), similar to typical galaxies at $z \simeq 8$. There is a clear flux density upturn in the F444W filter (relative to the neighboring shorter wavelength filters), suggesting either large EW [O III] emission (as expected for galaxies dominated by young stellar populations) or a

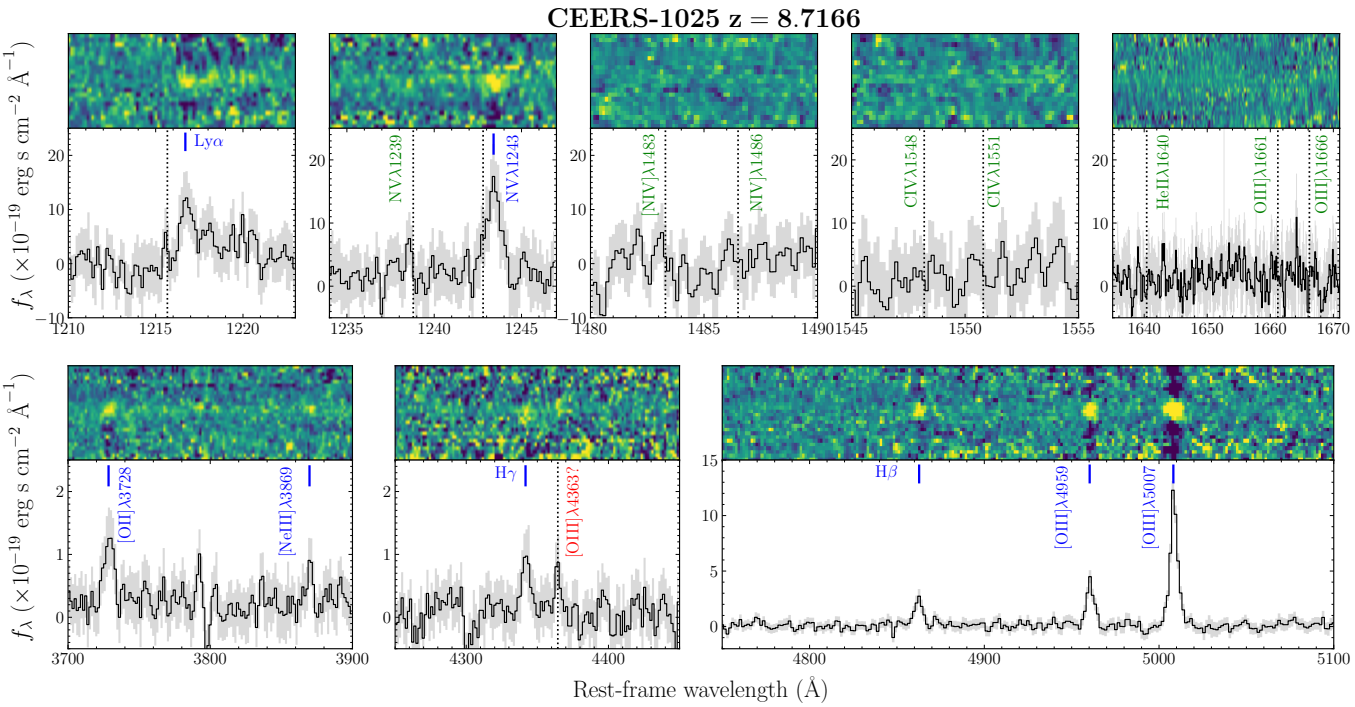

Figure 2. JWST/NIRSpec grating spectra of the N V emitter CEERS-1025. The top panels show the GO 4287 G140H spectra and the bottom panels show the composite GO 4287 and CEERS G395M spectra. We overplot the expected positions of emission lines from the systemic redshift ($z_{\rm sys} = 8.7166$) as black dotted lines. Detected emission lines are marked by blue solid lines. [O III] λ4363 is tentatively (S/N = 2.7) detected and marked by red text. Non-detections (N V λ1239, N IV], C IV, He II, O III]) are shown by green text.

reddened rest-frame optical continuum (as seen in many broad line AGN seen with *JWST*). The CEERS G395M spectrum confirms the former case, revealing very strong line emission ([O III]+Hβ EW $= 1493 \pm 93$ Å) seen in many $z \gtrsim 7$ galaxies.

The new G140H spectrum presented in this paper covers rest-frame wavelengths between 1000 Å and 1880 Å for CEERS-1025 (Figure 2), providing deeper and higher resolution rest-frame UV coverage and the first useful constraints blueward of 1245 Å. We present the new rest-frame UV spectrum in Section 3.1.1 before briefly discussing the newly-acquired rest-frame optical spectrum in Section 3.1.2. We will adopt a systemic redshift $z_{\rm sys} = 8.7166$ derived from the [O III] doublet and Hβ emission lines in the GO 4287 G395M spectrum, which is consistent with the redshift reported in Nakajima et al. (2023) and Tang et al. (2023).

3.1.1. *Rest-Frame UV Spectrum of CEERS-1025*

We visually search the rest-frame UV spectrum of CEERS-1025 (top panel of Figure 2) for emission lines. One feature is detected at an observed frame wavelength of 11822.9 Å (S/N = 5), near the rest-frame wavelength of Lyα. The only other robust emission feature detected in the rest-frame UV spectrum is at observed wavelength of 12081.6 Å (S/N = 6), close to the expected wavelengths of the N V $\lambda\lambda$1239, 1243 resonant doublet. If this feature is nebular N V emission, it would suggest CEERS-1025 powers a hard radiation field, with a supply of photons with energies > 77 eV capable of producing N V ions.

The peak flux of the Lyα emission line is redshifted by $+272 \pm 33$ km s^{-1} from Lyα resonance. The core of the Lyα line is narrow, but there is a red tail of emission extending to ~ 1000 km s^{-1}. The redshifted peak velocity and asymmetric profile of Lyα is consistent with the presence of outflowing neutral gas in CEERS-1025, as is commonly seen in high redshift galaxies. We cannot rule out the possibility that the extended red wing is associated with the broad line region of an AGN (with the blue side scattered by the IGM), but since no similar broad profile is seen for Hβ, we will assume that the asymmetric Lyα profile is more likely driven by with backscattering in a neutral outflow. The Lyα emission line of CEERS-1025 (and implications for the IGM) will be discussed in detail in Whitler et al. (2025, in prep).

The N V line is a doublet ($\lambda = 1238.8$ Å and $\lambda = 1242.8$ Å), but only one component is detected in our spectrum. The detected feature is narrow, with no clear broad component present in the existing spectrum. After de-convolving the instrument resolution, the de-

Table 2. Rest-frame UV to optical emission line EWs (Å) and 3σ upper limits of the two N V emitters.

	CEERS-1025	CEERS-7902
N V λ1239	< 2.7	27.9 ± 3.4
N V λ1243	7.0 ± 1.1	< 7.7
[N IV] λ1483	< 3.1	< 8.6
N IV] λ1486	< 3.3	< 8.6
C IV λ1548	< 3.9	< 8.7
C IV λ1551	< 3.3	< 9.2
He II λ1640	< 4.8	< 14
O III] λ1661	< 5.3	< 11
O III] λ1666	< 4.7	< 13
N III] λ1746	< 5.2	-
N III] λ1748	< 5.1	-
[C III] λ1907	-	< 19
C III] λ1909	-	22.5 ± 7.7
[O II] λ3728	39 ± 10	10 ± 6
[Ne III] λ3869	16 ± 6	20 ± 5
Hγ (total)	75 ± 21	33 ± 9
Hγ (narrow)	-	12 ± 4^{a}
Hγ (broad)	-	21 ± 8^{b}
[O III] λ4363	39 ± 15	22 ± 4
Hβ (total)	200 ± 34	141 ± 11
Hβ (narrow)	-	17 ± 3^{a}
Hβ (broad)	-	124 ± 10^{b}
[O III] λ4959	331 ± 35	52 ± 4
[O III] λ5007	1004 ± 44	155 ± 5
He I λ5877	-	17 ± 6
[O I] λ6302	-	11 ± 3

NOTE—a: Narrow component of the Hγ or Hβ emission line of CEERS-7902. b: Broad component of the Hγ or Hβ of CEERS-7902.

tected line has a full width at half maximum (FWHM) of 208 ± 28 km s^{-1}. The emission line is closest to the red component of the doublet, with a peak flux redshifted by $+144 \pm 32$ km s^{-1} from line center. In what follows, we will assume the feature is N V λ1243, but we note that we cannot immediately rule out that we are seeing the blue component at a very high velocity ($+1113 \pm 32$ km s^{-1}) from line center. As with Lyα, the redshifted N V profile is consistent with backscattering off of outflowing gas, but in this case, the presence of N V resonant scattering would indicate that the outflowing material has a very highly ionized component capable of scattering N V photons. We measure a line

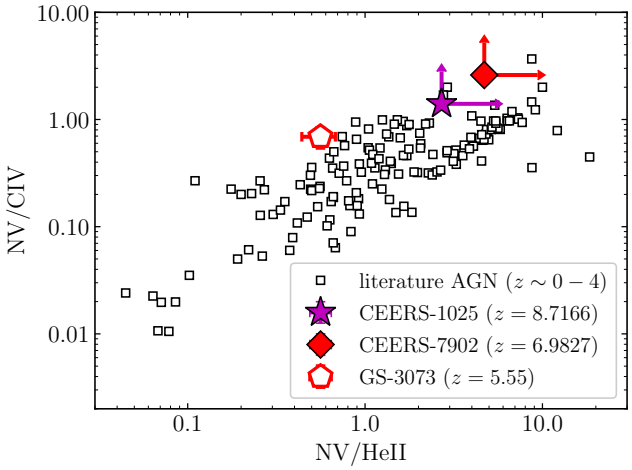

Figure 3. N V $\lambda\lambda$1239, 1243/C IV $\lambda\lambda$1548, 1551 versus N V $\lambda\lambda$1239, 1243/He II λ1640 diagnostic. The two N V emitters in GO 4287 are shown as magenta star (CEERS-1025, $z = 8.7166$) and red diamond (CEERS-7902, $z = 6.9827$, a LRD). We overplot the broad line AGN GS-3073 ($z = 5.55$; open red pentagon) from Ji et al. (2024). Open black squares show AGN from literature ($z \sim 0-4$; Kraemer & Crenshaw 2000; Baldwin et al. 2003; Kuraszkiewicz et al. 2004; Nagao et al. 2006a; Hainline et al. 2011; Matsuoka et al. 2011; Alexandroff et al. 2013; Dors et al. 2014).

flux of $1.40 \pm 0.23 \times 10^{-18}$ erg s^{-1} cm^{-2} and an associated rest-frame EW of 7.0 ± 1.1 Å.

The line ratios of resonant doublets (i.e., N V, C IV) can face significant radiative transfer effects, with the resulting line ratio depending on the column density and kinematics of the absorbing gas. The theoretical flux ratio of the doublet is $f_{\rm NV\lambda1239}/f_{\rm NV\lambda1243} = 2$ (Bickel 1969), assuming the level populations are dominated by collisional excitation. In the case that photon absorption dominates excitation, the doublet ratio becomes the ratio of Einstein A coefficients, yielding a flux ratio of $f_{\rm NV\lambda1239}/f_{\rm NV\lambda1243} = 1$. If we interpret the detected N V emission feature as the N V λ1243, we can place a 3σ upper limit on the N V λ1239 flux ($< 5.2 \times 10^{-19}$ erg s^{-1} cm^{-2}) and EW (< 2.7 Å). This would suggest the $f_{\rm NV\lambda1239}/f_{\rm NV\lambda1243}$ flux ratio in CEERS-1025 is < 0.37 (at 3σ), very different from the theoretical value ($1-2$), regardless of whether collisions or absorption dominates excitation.

One possible explanation for the observed doublet ratio could be the effect of N V photons scattering through highly ionized outflowing gas. In a simplified picture, the N V emission is produced by ions near (or close to) the systemic redshift (similar to the other narrow lines in the spectrum), but the line profile is then altered by resonant scattering through a highly ionized outflowing medium. The N V ions in the outflowing gas process

a redshifted version of the spectrum. As a result, the N V λ1243 transition in the outflow will preferentially scatter photons on the blue side of the N V λ1243 emission line emitted by the galaxy. The precise outcome will depend on the geometry, column density, and velocity profile of the outflowing gas. If there is sufficient opacity extending over the velocity separation of the doublet ($\sim$ 1000 km s^{-1}), this can lead to N V λ1239 photons being scattered away by the N V λ1243 transition in the outflowing gas. The N V λ1239 photons will additionally likely face self-absorption from the N V λ1239 transition in the outflowing gas. In contrast, the N V λ1243 photons would only face scattering from the N V λ1243 transition, as there is no redder component. In this case, the $f_{\rm NV\lambda1239}/f_{\rm NV\lambda1243}$ doublet ratio would decrease relative to the theoretical value. In reality the situation may be more complicated if the outflowing gas is not uniformly distributed (e.g., Wang et al. 2010). Nevertheless, the kinematics of outflowing gas has been suggested to play a role in C IV and Mg II line profiles (e.g., Chang & Gronke 2024; Topping et al. 2024a) and may be impacting the N V doublet in CEERS-1025. Confirmation of this scenario would require a deeper spectrum capable of detecting the velocity profile of highly ionized gas in absorption, or integral field spectroscopy capable of detecting the diffuse flux from the scattered component of the N V doublet. A higher S/N spectrum may also be expected to reveal broad emission in the detected N V λ1243 component if the outflow is scattering line photons up to $\sim$ 1000 km s^{-1}.

Assuming the N V emission in CEERS-1025 probes a hard radiation field, we may also expect to detect line emission from other highly-ionized species. The G140H observations cover N IV], C IV, He II, O III], N III], but none of these features is detected (Figure 2). The 3σ limits on flux ratios between N V and other UV lines are well above unity (N V/N IV] $>$ 1.4, N V/C IV $>$ 1.4, N V/He II $>$ 2.6). These flux ratios imply CEERS-1025 is a stronger nitrogen emitter than many AGN with narrow UV lines (where typically N V/C IV $<$ 1 and N V/He II $<$ 2, Figure 3; e.g., Nagao et al. 2006a; Hainline et al. 2011; Alexandroff et al. 2013; Ji et al. 2024). On the other hand, there are examples of AGN with similar N V/C IV ($\simeq 1-10$) and N V/He II ratios ($\simeq$ 2$-$10; e.g., Kraemer & Crenshaw 2000; Baldwin et al. 2003; Kuraszkiewicz et al. 2004; Jiang et al. 2008; Matsuoka et al. 2011; Dors et al. 2014), many of which have been described as nitrogen-loud systems (e.g., Baldwin et al. 2003; Jiang et al. 2008). We note that the nitrogen-enhanced line ratios tend to refer to broad lines, whereas here we are observing similar line ratios from narrow line emitting gas. What drives the nitrogen excess in these AGN is not clear. In some cases, such large N V/C IV and N V/He II ratios have been argued as a signpost of supersolar metallicities (e.g., Hamann & Ferland 1992; Baldwin et al. 2003; Nagao et al. 2006b), whereas others have suggested that a nitrogen enhanced abundance pattern may contribute (e.g., Ji et al. 2024). We will discuss potential implications of the line ratios further in Section 3.4.

Finally, we do note that the N V doublet is also ubiquitous in very hot stellar atmospheres, where it is most commonly encountered in P-Cygni profile prominent for O stars hotter than O6, corresponding to effective temperatures $\gtrsim$ 35 kK (e.g., Walborn & Panek 1984). It can also be produced in nearly pure emission in the hottest Wolf-Rayet atmospheres, where generally it is substantially broadened by the high velocities ($\gtrsim$ 1000 km s^{-1}) of the optically thick winds where it is produced (e.g., Hainich et al. 2014). While slower wind velocities are possible especially for very luminous/massive stars at extremely low metallicities (e.g., Vink 2022), 208 km s^{-1} (the FWHM of N V λ1243 of CEERS-1025) is extraordinarily low in the context of stellar winds. Crucially, it would also be atypical to encounter prominent N V without any of the other strong wind features commonly encountered alongside it: most notably, C IV and He II, as well as N IV] λ1486 and N IV λ1719. While we cannot entirely rule out a contribution from stellar winds, the requirements on these would be unusual.

3.1.2. *Rest-Frame Optical Emission Lines in CEERS-1025*

The composite rest-frame optical spectrum of CEERS-1025 (bottom panel of Figure 2) reveals a suite of strong lines ([O II], [Ne III], Hβ, [O III] λ4959, and [O III] λ5007), similar to that reported in the CEERS discovery spectrum (e.g., Tang et al. 2023). We additionally identify the tentative [O III] λ4363 auroral line (S/N = 2.5) which we will discuss below.

As was the case in the original spectrum of CEERS-1025, no broad emission lines are detected, either in the Balmer lines or the forbidden oxygen lines. We can constrain the flux of broad Hβ based on the non-detection. Assuming a line width that is typical in broad-line AGN (FWHM $\simeq$ 2000 km s^{-1}; e.g., Harikane et al. 2023; Kocevski et al. 2024; Maiolino et al. 2024a; Matthee et al. 2024; see also Section 4.2.2), the broad Hβ line flux is $< 5.0 \times 10^{-19}$ erg s cm^{-2} at 3σ. This indicates an upper limit on the broad-to-narrow Hβ flux ratio of $<$ 0.34, well below that is typical of broad-line AGN ($\simeq 1-2$; e.g., Harikane et al. 2023; Kokorev et al. 2023; Übler et al. 2023; Juodžbalis et al. 2024; Matthee et al. 2024). Although we cannot fully rule out the presence of a broad emission lines, the existing spectrum suggests

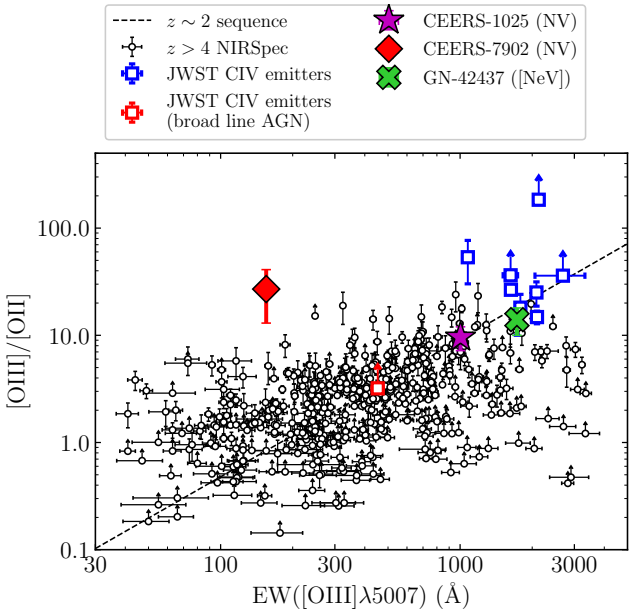

Figure 4. [O III] $\lambda\lambda 4959, 5007$/[O II] $\lambda 3727$ as a function of [O III] $\lambda 5007$ EW. We show the two N V emitters in GO 4287 CEERS-1025 as a magenta star and CEERS-7902 (LRD) as a red diamond. We overplot the [Ne V] $\lambda 3427$ emitter GN-42437 in Chisholm et al. (2024) as green cross. We also overplot C IV emitters in Topping et al. (2024a) and Topping et al. (2025a) as open blue squares, where the broad-line AGN is shown as the open red square. The full $z > 4$ spectroscopic sample is shown as open black circles. The relation derived from $z \sim 2$ galaxies (Tang et al. 2019) is shown as the black dashed line.

that CEERS-1025 is possibly a narrow line AGN with its broad line region obscured.

The observed Balmer decrement is consistent with minimal attenuation. We measure Hγ/H$\beta = 0.47 \pm 0.15$, which is consistent with the intrinsic Hγ/Hβ ratio expected from case B recombination (0.47, assuming the appropriate electron temperature, see below paragraphs; Osterbrock & Ferland 2006). As noted above, the UV continuum slope of CEERS-1025 is very blue, with $\beta = -2.5$, further suggesting minimal dust attenuation, as is common in $z \gtrsim 8$ galaxies. Based on these results, we do not correct the rest-frame optical emission lines for reddening.

Tang et al. (2023) concluded that the narrow rest-frame optical lines in CEERS-1025 appear broadly consistent with expectations for a galaxy dominated by a young stellar population (2 Myr assuming constant star formation history) formed in a recent burst with moderately low metallicity ([O III] $\lambda 5007$/Hβ flux ratio $= 4.4 \pm 0.8$). The [O III]+Hβ EW of CEERS-1025 is large (1535 ± 66 Å), with a value among the upper 10% of EWs observed at $z \simeq 6-9$ (Endsley et al. 2024). Such large [O III]+Hβ EWs are also linked to the strong nebular C IV emitters, thought to trace a population of metal poor massive star clusters (e.g., Topping et al. 2025a). In star forming galaxies, we expect ionization-sensitive flux ratios (i.e. [O III]/[O II], hereafter O32) to increase with the rest-frame optical emission line EWs (Tang et al. 2019; Sanders et al. 2020; Tang et al. 2023). Assuming zero dust attenuation, we find a large O32 value ($= 9.6 \pm 2.4$) that places CEERS-1025 on the same ionization vs. [O III]+Hβ EW sequence as star forming galaxies at high redshift (Figure 4). If an AGN is the source of the narrow N V emission in CEERS-1025, it is not altering the strong rest-frame optical line ratios and EWs in a manner that can be easily distinguished from what is seen in normal star forming galaxies.

An AGN power law spectrum should more efficiently heat the gas than a stellar ionizing spectrum, increasing the strength of auroral lines relative to hydrogen recombination lines (Brinchmann 2023; Mazzolari et al. 2024b; Übler et al. 2024). Mazzolari et al. (2024a) have developed a set of AGN diagnostics using a suite of photoionization models to derive a demarcation between AGN and stars using the combination of [O III] $\lambda 4363$/Hγ and [Ne III]/[O II] (hereafter Ne3O2) flux ratios. The detection of a tentative [O III] $\lambda 4363$ emission feature in the new composite G395M spectrum (Figure 2) is suggestive of a large [O III] $\lambda 4363$/Hγ ratio (0.53 ± 0.26) that would place CEERS-1025 firmly in the AGN regime based on the Mazzolari et al. (2024a) diagnostics (Figure 5). A deeper spectrum will be required to confirm this detection.

We can quantify the the physical properties that would be implied from the existing measurement of the auroral line strength. Using the `PYTHON` package `PyNeb` (Luridiana et al. 2015) and assuming an electron density $n_e \simeq 1000$ cm^{-3} that is typical at $z \sim 9$ (e.g., Isobe et al. 2023), we derive an electron temperature T_e(O III) $= 3.0^{+1.3}_{-0.9} \times 10^4$ K for the O^{++} zone. Because the auroral [O II] $\lambda\lambda 7320, 7330$ lines are not covered by the NIRSpec spectra and are likely very faint, we derive the O^+ zone electron temperature T_e(O II) using the relation T_e(O II) $= 0.7 \times T_e$(O III) +3000 K (Campbell et al. 1986; Garnett 1992). Combining with the [O III] $\lambda 5007$/Hβ and [O II]/Hβ ratios, this indicates a gas-phase oxygen abundance $12 + \log(\mathrm{O/H}) = 7.18^{+0.24}_{-0.10}$ ($Z_{\rm neb} = 0.03^{+0.02}_{-0.01}\ Z_\odot$, solar metallicity corresponds to $12 + \log(\mathrm{O/H}) = 8.71$; Gutkin et al. 2016). While the inferred electron temperature and oxygen abundance remains mostly unchanged over a wide electron density range $n_e = 10^2 - 10^4$ cm^{-3}, the calculated values would be different at yet higher electron densities seen in compact star forming galaxies (e.g., Topping et al.

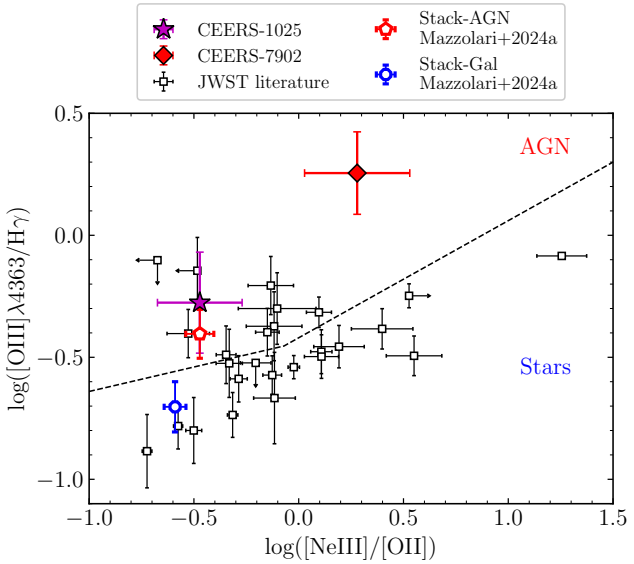

Figure 5. [O III] λ4363/Hγ versus [Ne III] λ3869/[O II] diagnostics, with black dashed line showing the demarcation between galaxies dominated by stars and AGN (Mazzolari et al. 2024b). We show the two N V emitters CEERS-1025 as magenta star and CEERS-7902 (LRD) as red diamond. We overplot galaxies with [O III] λ4363 detections from literature *JWST* studies (Nakajima et al. 2023; Hu et al. 2024; Sanders et al. 2024; Topping et al. 2024a, 2025a) in open black squares, as well as the stacked narrow line AGN (open red pentagon) and stacked galaxies (open blue octagon) from (Mazzolari et al. 2024a).

2024a, 2025a). At $n_e \simeq 10^5$ cm^{-3}, the inferred electron temperature decreases to $= 2.4^{+0.9}_{-0.7} \times 10^4$ K and the oxygen abundance becomes $12 + \log(\mathrm{O/H}) = 7.75^{+0.32}_{-0.24}$ ($Z_{\rm neb} = 0.11^{+0.12}_{-0.05}$ $Z_\odot$). While there is still considerable uncertainty in these measurements, the results suggest that the gas in CEERS-1025 is likely fairly metal poor.

3.2. *Spectroscopy of $z = 6.99$ galaxy CEERS-7902*

CEERS-7902 (R.A. = 214.983038, Decl. = +52.956205) is a broad line AGN that is relatively faint in the rest-frame UV continuum ($m_{\rm F115W} = 27.0$, $\mathrm{M_{UV}} = -19.9$). The NIRCam photometry and initial characterization of this object was presented in Labbé et al. (2023), identifying that CEERS-7902 (ID 38094 in their analysis) has a very red rest-frame optical SED ($\beta_{\rm opt} = 0.89$; Kocevski et al. 2024), consistent with the LRD population. CEERS-7902 does not exhibit a significant UV upturn; instead its UV slope remains fairly red ($\beta_{\rm UV} = -0.75$) (see right panel of Figure 1).

A low-resolution ($R \sim 100$) NIRSpec prism spectrum and medium-resolution G395M/F290LP spectrum of CEERS-7902 was obtained in RUBIES. The RUBIES spectrum of CEERS-7902 (ID 55604 in RUBIES) confirmed the presence of broad Hβ emission with narrow forbidden lines (Kocevski et al. 2024; Wang et al. 2024b), leading to its characterization as a broad line AGN at $z = 6.99$, as reported in Kocevski et al. (2024). That paper also notes the presence of a narrow absorption line in the Hβ profile (blueshifted from line center), as has been seen in $10-20\%$ of Type I AGN discovered with *JWST* (e.g., Juodžbalis et al. 2024; Kocevski et al. 2024; Labbe et al. 2024; Lin et al. 2024; Matthee et al. 2024; Wang et al. 2024b,a). This may indicate the presence of neutral gas with sufficient density ($\gtrsim 10^8$ cm^{-3}) to populate the $n = 2$ level of hydrogen. Using local scaling relations (Greene & Ho 2005), Kocevski et al. (2024) infer a black hole mass of $M_{\rm BH} = 2.0 \times 10^9$ $M_\odot$ (after correcting for dust attenuation of the optical continuum). By jointly fitting AGN and stellar contributions to the SED, they infer a stellar mass of $M_\star = 1.3 \times 10^{10}$ $M_\odot$ and an optical attenuation of $A_V = 3.4$, similar to the values reported in Wang et al. (2024b) ($M_\star = 6.2 \times 10^9$ $M_\odot$ and $A_V = 3.8$).

Here we present the first deep rest-frame UV view of CEERS-7902 at high resolution using the G140H grating (Figure 6) and a new moderate resolution G395M spectrum targeting the rest-frame optical. Below we describe the rest-frame UV emission line measurements (Section 3.2.1). We then briefly comment on the rest-frame optical spectra of CEERS-7902 (Section 3.2.2). In the following, we adopt a systemic redshift of $z_{\rm sys} = 6.9827$ derived from the narrow [O III] doublet and other strong forbidden lines in the composite G395M spectrum. This value is consistent with that measured for similar lines in the RUBIES grating spectrum of this galaxy.

3.2.1. *Rest-Frame UV Emission Lines in CEERS-7902*

We visually search the G140H spectrum (top panel of Figure 6) for emission lines, identifying a strong (8σ) feature at 9892.4 Å, close to the expected position of N V λ1239. We also find another confidently-detected (3σ) emission line at 15238.0 Å, consistent with the expected wavelength of the red component of the [C III], C III] $\lambda\lambda$1907, 1909 doublet. As described below, both detected UV lines are narrow. Broad lines with FWHM similar to the broad Hβ seen in the rest-frame optical are not detected in the rest-frame UV spectrum of CEERS-7902.

The emission feature seen near the N V resonance could either be interpreted as the blue component of the N V doublet, with peak flux emerging slightly redshifted ($+104 \pm 39$ km s^{-1}) from line center, or it could be interpreted as the red component of the N V doublet with its peak flux significantly blueshifted (-861 ± 39 km s^{-1}). The observed line width of N V λ1239 emission (FWHM $= 101 \pm 25$ km s^{-1}) is similar to the instrument res-

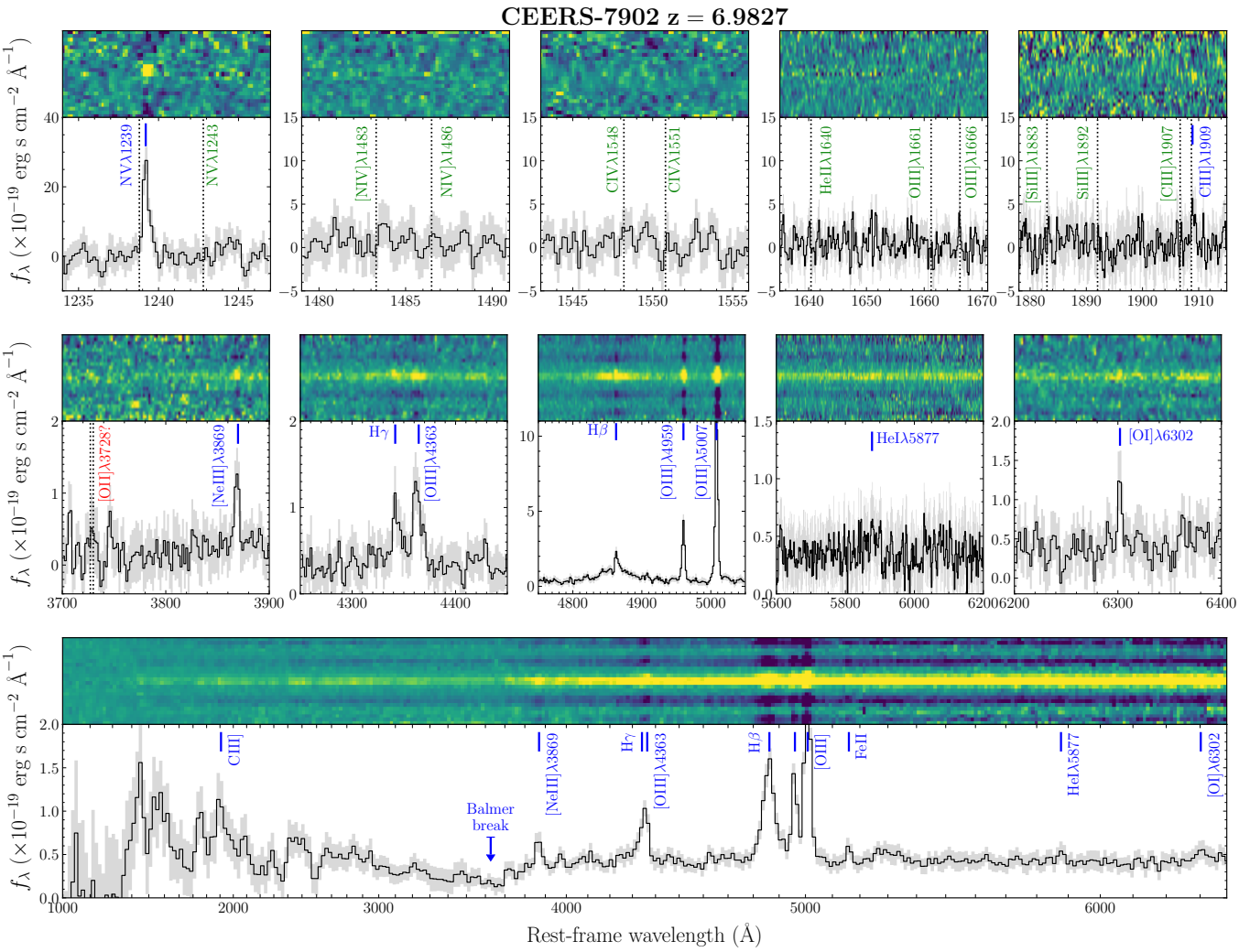

Figure 6. NIRSpec spectra of the N V emitter CEERS-7902 (LRD). We show the GO 4287 G140H, the composite of GO 4287 and RUBIES G395M, and the RUBIES prism spectra from top to bottom. Spectra are shown in the same way as Figure 2. We find tentative detection of unresolved [O II] λ3728 emission line (S/N = 2), which is marked by red text.

olution ($\simeq$ 111 km s^{-1}), suggesting that the N V-emitting gas is kinematically distinct from the gas in the broad line region of the AGN. The measured flux ($1.20 \pm 0.15 \times 10^{-18}$ erg s^{-1} cm^{-2}) suggests an EW of 27.9 ± 3.4 Å. Here we find the same EW value regardless of whether we use the stacked flux density in the spectrum or the NIRCam-measured rest-frame UV flux density underneath the emission line.

We note that the detected feature near N V is redshifted by $\simeq$ 5800 km s^{-1} from Lyα. While it is conceivable that we are seeing Lyα that has been shifted in wavelength greatly owing to interaction with a very dense (and dust-free) column of hydrogen, we would expect to see a broadened line profile in this case, not the narrow line in the spectrum. In what follows, we will assume that the detected feature in CEERS-7902 is nebular emission associated with the N V doublet, likely implying photoionization from a source of 77 eV photons. As noted in Section 3.1.1, if the detected N V feature was associated with stellar winds, we would expect to see other lines (i.e., C IV, He II, N IV]) not present in the spectrum.

Only one of the N V components is detected in the existing spectrum. We place a 3σ EW upper limit on the undetected component of $<$ 7.7 Å. If we assume the observed line is N V λ1239, it would imply a doublet flux ratio limit of $f_{\rm NV\lambda1239}/f_{\rm NV\lambda1243} > 3.7$ (3σ), much larger than the theoretically expected range of $1-2$. In the case that the detected feature is highly blueshifted emission from N V λ1243, it would imply a line ratio ($f_{\rm NV\lambda1239}/f_{\rm NV\lambda1243} < 0.27$ at 3σ) that is also inconsistent with theoretical values. As discussed in Section 3.1.1, line ratios of resonant doublets can be impacted by scattering. To preferentially boost the blue

component would require scattering through infalling material. This picture does not provide a fully satisfactory explanation of the line profile, as we will discuss in Section 3.4.

The gas clouds responsible for the N V emission appear to not emit strongly in C IV or He II. We place 3σ upper limits on the fluxes and EWs of N IV], C IV, He II, O III], and N III]. The flux ratios between N V and other UV lines are well above unity, with N V/N IV] > 2.4, N V/C IV > 2.6, and N V/He II > 4.8. While these line ratios are not typical (e.g., Nagao et al. 2006a; Alexandroff et al. 2013; Hainline et al. 2011; Ji et al. 2024), they are consistent with those found in some populations of AGN, including many nitrogen-loud AGN (e.g., Kraemer & Crenshaw 2000; Baldwin et al. 2003; Kuraszkiewicz et al. 2004; Jiang et al. 2008; Matsuoka et al. 2011; Dors et al. 2014; Figure 3, see also Section 3.1.1).

The detection of the C III] λ1909 emission line provides further insight into the gas conditions associated with CEERS-7902. The line is narrow, with FWHM $= 135 \pm 36$ km s^{-1}, similar to the line width of N V as well as the other narrow lines in the rest-frame optical. The emission feature has a peak consistent with line center ($+28 \pm 26$ km s^{-1}), using the systemic redshift implied by the forbidden lines in the rest-frame optical. The measured flux ($3.5 \pm 1.2 \times 10^{-19}$ erg s^{-1} cm^{-2}) indicates a rest-frame EW of 22.5 ± 7.7 Å. Such a large value (for an individual C III] component) is rarely seen in star forming galaxies (e.g., Shapley et al. 2003; Stark et al. 2014, 2015a; Hutchison et al. 2019; Du et al. 2020; Mainali et al. 2020; Tang et al. 2021; Roberts-Borsani et al. 2024) but is commonly exhibited by AGNs (Nakajima et al. 2018; Le Fèvre et al. 2019). The doublet flux ratio constrains the density of the C III]-emitting gas. The absence of the the [C III] λ1907 line implies a limit of $f_{\mathrm{CIII}]\lambda1909}/f_{[\mathrm{CIII}]\lambda1907} > 1.2$ at 3σ. Using `PyNeb` and assuming an electron temperature $T_e = 4 \times 10^4$ K, we derive an electron density of $n_e > 3 \times 10^4$ cm^{-3} from the doublet ratio. Such high densities are not uncommon in gas traced by the C III] doublet at high redshift (e.g., Maiolino et al. 2024b; Senchyna et al. 2024; Topping et al. 2024a, 2025a,b).

O I emission lines are often seen in in AGN spectra (e.g., Grandi 1980; Rodríguez-Ardila et al. 2002; Riffel et al. 2006; Martínez-Aldama et al. 2015; Cracco et al. 2016; Juodžbalis et al. 2024; Wang et al. 2024a). The strength of three of these lines (1304, 8446, and 11287 Å) can be boosted significantly by Lyβ pumping, owing to the similarity of the Lyβ resonance wavelength and that of the $3d^3$ D^0 excited state of the O I atom (Kwan & Krolik 1981), the decay of which produces O I photons with the aforementioned wavelengths. Several *JWST*-detected AGNs have shown the two reddest O I lines, but confirmation of the Lyβ fluorescence picture requires detection of the 1304 Å line. CEERS-7902 should be a candidate for Lyβ pumping of the O I transitions owing to the indications of extremely dense gas from Hβ absorption (and potentially the Balmer break). However we do not see the O I λ1304 in the spectrum, and the two redder transitions associated with Lyβ pumping are not covered by existing spectroscopy. We place a 3σ upper limit of 3.1×10^{-19} erg s^{-1} cm^{-2} on the line flux of O I λ1304. The absence of the line is likely related in part to the strong reddening that is present in the rest-frame UV of CEERS-7902. A considerably deeper spectrum would be required to usefully test the existence of the O I transitions.

3.2.2. *Rest-Frame Optical Emission Lines in CEERS-7902*

The composite G395M spectrum of CEERS-7902 (middle panel of Figure 6) reveals a suite of rest-frame optical emission lines ([Ne III], Hγ, Hβ, and [O III]). The Hβ line shows a broad emission component with a narrow absorption feature (Kocevski et al. 2024; Wang et al. 2024b). Broad emission is also seen in He I λ5877 in the G395 spectrum. We additionally detect narrow emission at the expected wavelengths of [O III] λ4363 (S/N = 5), and we detect unresolved [O II] λ3728 doublet (S/N = 2) as well as [O I] λ6302 (S/N = 4) in the G395 spectrum. We also detect a tentative emission near [Fe VII] λ5159 (S/N = 1.5).

We simultaneously fit the narrow and broad Hβ emission profile with two Gaussians. We derive FWHMs of 274 ± 40 km s^{-1} (narrow) and 3560 ± 210 km s^{-1} (broad). We find a similar FWHM for the broad He I λ5877 component (2731 ± 635 km s^{-1}). The spectral width of the broad Hβ component is consistent to that measured in Wang et al. (2024b) from RUBIES G395M spectrum (FWHM $= 3595 \pm 250$ km s^{-1}). It is lower than that presented in Kocevski et al. (2024) (FWHM $= 4870 \pm 480$ km s^{-1}). A higher S/N spectrum should yield a more robust measure, but for the purposes of this paper, the precise width of the broad component is not critical. We also characterize the Hβ absorption feature reported in the literature (Kocevski et al. 2024; Wang et al. 2024b). The absorption is strong (EW $= -3.3$ Å), narrow (FWHM $= 334$ km s^{-1}), and slightly blueshifted with respect to the line center (-321 km s^{-1}). The rest-frame optical spectrum of CEERS-7902 also shows a Balmer break (bottom panel of Figure 6) which could either be due to stars (Wang et al. 2024b) or Balmer limit absorption from dense gas (e.g., Inayoshi & Maiolino 2025; Ji et al. 2025).

Interpretation of narrow lines requires insight of whether they are significantly reddened by dust. The rest-frame optical spectrum of CEERS-7902 shows detection of narrow Hγ and Hβ emission, allowing us to measure the Balmer decrement of the narrow line emitting gas. We simultaneously fit the narrow and broad Hγ emission as well as [O III] λ4363 with three Gaussians, fixing the line width of the broad Hγ to the value derived from broad Hβ. From this, we find that the narrow line Balmer decrement is Hγ/H$\beta = 0.67 \pm 0.27$. If there was significant reddening of the narrow lines, we would expect the ratio to be significantly lower than the intrinsic ratio expected from case B recombination (0.47; Osterbrock & Ferland 2006). The fact that we measure a value that is larger than intrinsic (albeit consistent within 1σ) gives no strong evidence that the narrow line emitting gas is strongly impacted by dust, although we note there may be deviations from case B (e.g., McClymont et al. 2024; Scarlata et al. 2024). In the following, we will not correct the narrow lines for reddening.

The narrow [O III]λ5007 line is the strongest line in the spectrum ($5.77 \pm 0.17 \times 10^{-18}$ erg s^{-1} cm^{-2}), but the derived rest-frame optical [O III] λ5007 EW ($= 155 \pm 5$ Å) is well below average at $z \simeq 6-9$ (e.g., Endsley et al. 2024). The line ratio between [O III] λ5007 and the narrow component of Hβ in CEERS-7902 is 9.8 ± 1.9, larger than typically seen in star-forming galaxies at similar redshifts (e.g., Sanders et al. 2023; Shapley et al. 2023, 2025; Trump et al. 2023; Backhaus et al. 2024; Kumari et al. 2024), The ionization-sensitive flux ratios are also large. The Ne3O2 ratio ($= 1.9 \pm 1.1$) of CEERS-7902 is larger than that of the vast majority of galaxies at high redshift (e.g., Cameron et al. 2023b; Nakajima et al. 2023; Shapley et al. 2023; Tang et al. 2023; Trump et al. 2023; Backhaus et al. 2024; Hu et al. 2024; Sanders et al. 2024; Shapley et al. 2025). The O32 ratio ($= 27 \pm 14$) also points to gas under extreme ionization conditions. Such large Ne3O2 and O32 ratios are rarely seen in galaxies with as low [O III] EW as is seen in CEERS-7902 (Figure 4). This likely reflects the additional contribution of the AGN continuum to the rest-frame optical, reducing the [O III] EW relative to systems dominated by stellar continuum.

The detection of [O III] λ4363 feature allows us to apply the diagnostics presented in Mazzolari et al. (2024b) to the narrow line gas in CEERS-7902. The measured narrow line [O III] λ4363/Hγ ratio (1.8 ± 0.7) is much larger than the limits implied by other galaxies in GO 4287 and by other galaxies with [O III] λ4363 detections in earlier *JWST* programs (e.g., Nakajima et al. 2023; Hu et al. 2024; Mazzolari et al. 2024a; Sanders et al. 2024; Topping et al. 2024a, 2025a). The [O III] λ4363/Hγ and [Ne III]/[O II] line ratios place CEERS-7902 in the regime expected for AGN in the models presented in Mazzolari et al. (2024b) (Figure 5). Although galaxies dominated by massive stars with large densities ($n_e \gtrsim 10^5$ cm^{-3}) could also have high [O III] λ4363/Hγ ratios, such large densities will result in weaker [O II], resulting in very large Ne3O2 and O32 ratios (e.g., Topping et al. 2024a, 2025a). The combination of large [O III] λ4363/Hγ and relatively low O32 and Ne3O2 in CEERS-7902 is consistent with expectations for AGN photoionization.

The tentative [O I] λ6302 emission line may also point to the presence of AGN photoionization. Because Hα is shifted out of the G395M spectrum, we estimate the Hα flux from the observed narrow Hβ flux assuming the case B value, Hα/Hβ = 2.76 (Osterbrock & Ferland 2006). The estimated narrow Hα line flux is 1.62×10^{-18} erg s^{-1} cm^{-2}. This indicates an [O I] λ6302/Hα ratio $= 0.27 \pm 0.09$ for the narrow line emitting gas. Together with the [O III] λ5007/Hβ ratio (= 9.8 for the NLR), these line ratios suggest the the gas in CEERS-7902 that emits in narrow lines is in the AGN regime of the diagnostics in Mazzolari et al. (2024a). The [O I] λ6302/Hα ratio is $\simeq 10\times$ larger than the typical value of stars at fixed [O III] λ5007/Hβ ratio.

3.3. *Spectroscopy of $z = 6.68$ galaxy CEERS-10444*

We present the rest-frame UV and optical spectra of CEERS-10444 (R.A. = 214.892231, Decl. = +52.877651). This system is relatively faint in the rest-frame UV continuum ($m_{\rm F115W} = 26.9$, $M_{\rm UV} = -19.9$). The NIRCam photometry of CEERS-10444 was presented in Kocevski et al. (2024), identifying that it has a red rest-frame optical SED ($\beta_{\rm opt} = 0.43$) that is consistent with the LRD population. Both a NIRSpec prism spectrum and NIRSpec G395M/F290LP spectrum were obtained in RUBIES (ID 49140 in RUBIES) and discussed in Kocevski et al. (2024) and Wang et al. (2024b). The RUBIES spectra show broad Hα and Hβ emission as well as narrow forbidden lines, leading to its characterization as a broad line AGN at $z = 6.68$. Similar to CEERS-7902, narrow absorption lines are also present in the Hα and Hβ profiles of CEERS-10444 (Kocevski et al. 2024; Wang et al. 2024b), likely indicating the presence of dense neutral gas populating the $n = 2$ level of hydrogen (Inayoshi & Maiolino 2025). Balmer break is shown in the RUBIES prism spectrum of CEERS-10444. We measure a Balmer break strength $f_{\nu,4050}/f_{\nu,3670} = 3.4 \pm 0.5$, which is consistent with that measured in Wang et al. (2024b) within 2σ (2.44 ± 0.10).

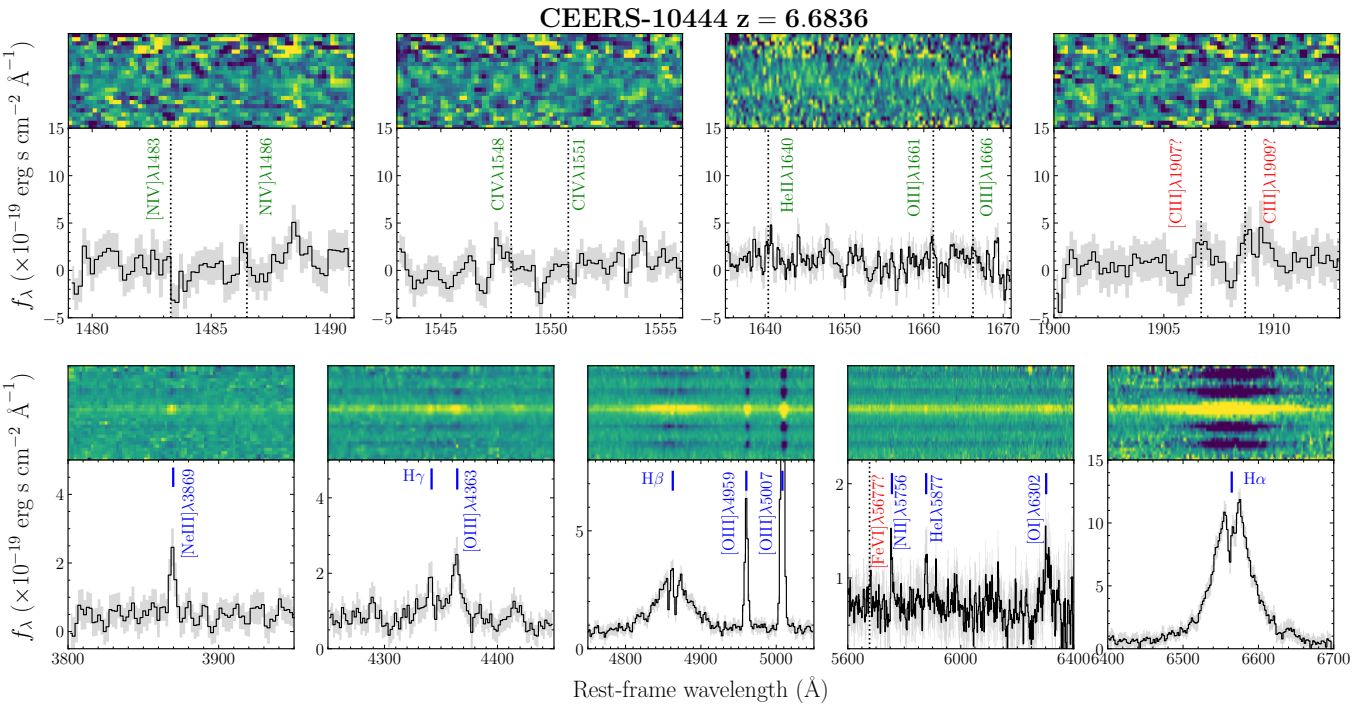

Figure 7. NIRSpec spectra of CEERS-10444 (LRD). We show the GO 4287 G140H spectrum in the top panel and the composite G395M spectrum (stacking the GO 4287 and RUBIES grating spectra) in the bottom panel. Spectra are shown in the same way as Figure 2.

In the top panel of Figure 7, we present the first deep, high-resolution rest-frame UV spectrum of CEERS-10444 from GO 4287 with G140H. We also generate a composite G395M spectrum of CEERS-10444 (bottom panel of Figure 7) by stacking the GO 4287 and RUBIES G395M spectra. Using the narrow [O III] doublet and other strong forbidden lines in the composite G395M spectrum, we derive a systemic redshift of $z_{\rm sys} = 6.6836$. This is consistent with the redshift measured using the RUBIES grating spectrum (Kocevski et al. 2024; Wang et al. 2024b). In this subsection we will adopt this systemic redshift for CEERS-10444.

3.3.1. *Rest-Frame UV Emission Lines in CEERS-10444*

The G140H spectrum covers between 0.98 and 1.80 μm, corresponding to 1275 to 2345 Å in the rest-frame (top panel of Figure 7). We visually search for rest-frame UV emission lines in the G140H spectrum. We tentatively identify two emission lines at 14651.7 Å (2σ) and 14667.3 Å (3σ), respectively. They are consistent with the expected wavelengths of the [C III], C III] $\lambda\lambda$1907, 1909 doublet, with the peak of the blue (red) emission component $+28 \pm 27$ km s^{-1} ($+33 \pm 27$ km s^{-1}) away from the line center of [C III] λ1907 (C III] λ1909). Both lines are narrow, with FWHM $= 127 \pm 27$ km s^{-1} for [C III] λ1907 and FWHM $= 214 \pm 27$ km s^{-1} for C III] λ1909, similar to that of narrow forbidden lines in rest-frame optical. The measured fluxes ($f_{\rm [CIII]\lambda1907} = 1.6 \pm 0.8 \times 10^{-19}$ erg s^{-1} cm^{-2}, $f_{\rm CIII]\lambda1909} = 4.0 \pm 1.2 \times 10^{-19}$ erg s^{-1} cm^{-2}) indicate rest-frame EW $= 4.8 \pm 2.4$ Å for [C III] λ1907 and $= 11.6 \pm 3.6$ Å for C III] λ1909. Using the doublet flux ratio ($f_{\rm CIII]\lambda1909}/f_{\rm [CIII]\lambda1907} = 2.4 \pm 1.4$), we can constrain the density of the C III]-emitting gas. Using `PyNeb` and assuming an electron temperature $T_{\rm e} = 5.5 \times 10^4$ K (see Section 3.3.2), we derive a large electron density $n_{\rm e} = 1.6^{+1.3}_{-1.1} \times 10^5$ cm^{-3}.

We do not detect either C IV or He II in the G140H spectrum of CEERS-7902. We place 3σ upper limits on the EWs of EW$_{\rm CIV\lambda1548} < 5.8$ Å, EW$_{\rm CIV\lambda1551} < 6.6$ Å, and EW$_{\rm HeII\lambda1640} < 6.4$ Å. The N V doublet is not covered by the G140H spectrum so we cannot verify if the line is present. We verify that the other nitrogen-based lines in the rest-frame UV ([N III] and N IV]) are not present in the spectrum of CEERS-10444, with 3σ upper limits of < 8.6 and < 8.0 Å. We note that the tentative detection of C III] and non-detection of C IV and He II is consistent with what was seen in CEERS-7902, so it is plausible that both LRDs have similar rest-frame UV spectra. A bluer spectrum is required to test this possibility, verifying the strength of the N V doublet.

3.3.2. *Rest-Frame Optical Emission Lines in CEERS-10444*

The composite G395M spectrum of CEERS-10444 (bottom panel of Figure 7) reveals a suite of strong rest-

frame optical emission lines ([Ne III], Hγ, Hβ, [O III], Hα). Both Hβ and Hα show broad emission components with absorption features (see also Kocevski et al. 2024; Wang et al. 2024b). Broad emission is also seen in Hγ. We additionally detect narrow [O III] λ4363 emission (S/N = 5), narrow [N II] λ5756 emission (S/N = 4), and narrow He I λ5877 emission (S/N = 4). We detect a slightly broadened [O I] λ6302 emission line (S/N = 5). We also report several tentative iron emission lines (S/N $\simeq$ 2). We detect tentative emission near [Fe II] λ4288, blended O II λ4416+Fe II λ4418, [Fe VII] λ5159, Fe II λ5199, and [Fe VI] λ5677, which are often found in type I AGN (e.g., Dong et al. 2010; Rose et al. 2015). The [O II] doublet is shifted out of the blue end of the G395M spectrum.

The Hβ emission of CEERS-10444 shows a broad component and two absorption components. We simultaneously fit the broad and the two absorption profiles of Hβ with three Gaussians. For the broad component we derive FWHM = 3203 ± 112 km s^{-1}, which is consistent to that measured in Wang et al. (2024b) with the RUBIES G395M spectrum (FWHM = 3301 ± 173 km s^{-1}). The two Hβ absorption features are blueward (-301 km s^{-1}) and redward ($+226$ km s^{-1}) the systemic redshift, respectively. The blueshifted Hβ absorption is strong (EW = -6.6 Å) and narrow (FWHM = 68 km s^{-1}). The redshifted Hβ absorption is even stronger (EW = -8.2 Å) with a slightly wider profile (FWHM = 213 km s^{-1}). We note that it is possible that this is a single absorption feature near line center (similar to that presented in Naidu et al. (2025) with a narrow emission line filling in the center ($v = -61 \pm 116$ km s^{-1} away from the line center), creating the appearance of two absorption features.

The Hα profile of CEERS-10444 appears mostly similar to Hβ, with a broad emission component and strong absorption. We simultaneously fit the Hα profile with two Gaussians. For the broad component we derive FWHM = 2686 ± 39 km s^{-1}, roughly consistent with the line width of the broad Hβ emission. The Hα absorption is strong (EW = -30 Å), narrow (FWHM = 244 km s^{-1}), and blueshifted to the line center (-109 km s^{-1}). There is potentially a faint narrow emission line near line center ($v = +73 \pm 86$ km s^{-1}) that has been almost entirely filled in, similar to the central emission feature seen in Hβ. A higher resolution and higher S/N spectrum would help better characterize the line profile.

The Hγ of CEERS-10444 shows a broad and a narrow emission components. The broad component is blended with the auroral [O III] λ4363 line. We simultaneously fit the broad and narrow Hγ as well as [O III] λ4363 profiles with three Gaussians. The broad Hγ has a line width (FWHM = 4169 ± 613 km s^{-1}) consistent with that of Hβ. The measured narrow line [O III] λ4363/Hγ ratio (2.8 ± 1.3) is very large, consistent with many AGNs (see Figure 5). The detection of [O III] λ4363 allows us to infer the electron temperature. The measured [O III] λ4363/[O III] λ5007 ratio of CEERS-10444 is 7.8 ± 1.7. Using `PyNeb` and assuming the electron density $n_e = 1.6 \times 10^5$ cm^{-3} (as computed from the [C III], C III] doublet flux ratio), we derive an electron temperature of $T_e = 5.5^{+5.5}_{-2.0} \times 10^4$ K.

The [N II] λ5755 auroral line is narrow (FWHM = 319 ± 60 km s^{-1}). As [N II] λ5755 is usually faint, the detection of [N II] λ5755 in the spectrum of CEERS-10444 (EW = 6.5 ± 1.6 Å) may suggest a high electron temperature in the low-ionization gas. Unfortunately [N II] λ6584 emission is blended with the broad, strong Hα emission, preventing us to compute a temperature based on the [N II] λ5755/[N II] λ6584 ratio. The He I λ5877 emission is relatively narrow (FWHM = 439 ± 87 km s^{-1}) compared to broad Balmer emission lines. As the line is permitted, we expect there to be a broad component similar to that seen in CEERS-7902 (see Section 3.2.2). It is likely that the broad He I emission has a low S/N and thus is not clearly detected in the spectrum.

The [O I] λ6302 emission line is strong, as is commonly expected in the partially ionized regions of AGN. For the other LRD in our sample, CEERS-7902, we demonstrated that the [O I] λ6302/Hα ratio is consistent with that seen in many AGN spectra. We cannot measure the [O I] λ6302/Hα ratio for CEERS-10444 since we do not detect the narrow component of the Balmer lines. We do note that the [O I] λ6302 actually appears somewhat broader than the narrow forbidden lines ([O III], [N II]), with FWHM = 1132 ± 176 km s^{-1}. The [O I] line is narrower than the broad Balmer emission lines, as we expect since the critical density of [O I] λ6302 is not large enough for the line to trace the dense broad line region. Deeper data are required to confirm the broadening of [O I] λ6302 and its physical origin.

The [Fe VI] $\lambda\lambda$5146, 5677 doublet is sensitive to the electron temperature. While we tentatively detect the red component of the doublet, we do not detect the blue component. We place a 3σ lower limit on the [Fe VI] λ5677/[Fe VI] λ5146 line ratio > 0.74. Using `PyNeb` and assuming the electron density $n_e = 1.6 \times 10^5$ cm^{-3} inferred from [C III], C III] doublet flux ratio, we find that the observed [Fe VI] λ5677/[Fe VI] λ5146 ratio is consistent with that is expected (0.86) from the electron temperature inferred from [O III] λ4363 ($T_e = 5.5 \times 10^4$ K).

To summarize, CEERS-10444 is an LRD with a rest-frame optical spectrum that is similar in some respects to CEERS-7902, with both having broad hydrogen Balmer lines with strong absorption features. The rest-frame UV spectrum of CEERS-10444 shows [C III], C III] but not C IV or He II, as is also seen in CEERS-7902. However our G140H spectrum does not extend down to rest-frame 1240 Å in CEERS-10444, so we cannot verify if this source powers strong N V emission.

3.4. *Interpretation of Line Ratios*

We have detected the likely presence of narrow N V emission in two of the galaxies observed as part of GO 4287, CEERS-1025 and CEERS-7902. Both systems are undetected in C IV and He II, with limits indicating elevated N V/C IV and N V/He II ratios. One of the two galaxies (CEERS-7902) is a known broad line AGN with an SED consistent with most LRD selections. In this section, we consider what the line ratios may be revealing about these sources. We will focus on the highest ionization lines in the new rest-frame UV spectra as those are most likely to not have contribution from stars. Our goal in this section is primarily to investigate the range of factors that might adjust the N V-based line ratios and not to derive the specific properties of the two N V emitters.

We first consider whether the N V/He II and N V/C IV line ratios are plausibly consistent with expectations for photoionization from narrow line regions of AGN. In doing so, we use the set of updated Feltre et al. (2016) photoionization models as presented in Mignoli et al. (2019), developed using the version of `CLOUDY` presented in Ferland et al. (2013). The original Feltre et al. (2016) model grid assumes a fixed relation between the AGN luminosity and the distance of the gas cloud from the central source, with an inner radius of 300 pc for an AGN luminosity of 10^{45} erg s^{-1}. Reducing this inner radius at a fixed AGN luminosity leads to an increase in radiation pressure. We consider an updated version of the original Feltre et al. (2016) model grid, which includes turbulent velocity of 100 km s^{-1} and a smaller inner radius of 90 pc (see Hirschmann et al. 2019; Mignoli et al. 2019; Vidal-García et al. 2024). We summarize the main adjustable parameters below, but for full details the reader is directed to Feltre et al. (2016). The emitted spectrum from the AGN accretion disk is assumed to have a power law, going as $f_\nu \propto \nu^\alpha$ between $\lambda = 0.001$ and 0.25 μm. We will first consider $\alpha = -2.0$ (an arbitrary choice), but we will investigate the impact of allowing α to vary. We note that Feltre et al. (2016) use $\alpha = -1.2$ to $\alpha = -2.0$ and note that $\alpha = -1.7$ was inferred as the slope blueward of Lyα in the stacked spectrum of 53 quasars at $z \simeq 2.3$ (Lusso et al. 2015). The ionization parameter (U_S) is also an adjustable parameter in the models, defined at the Stromgren radius of the nebula. The hydrogen number density (n_H) and gas metallicity (Z) are additional free parameters. The heavy element abundances ratios are the same as those adopted in Gutkin et al. (2016) and Feltre et al. (2016), largely based on Caffau et al. (2011) for the solar abundance scale. All element abundances except for nitrogen are assumed to scale linearly with the oxygen abundance. The relative nitrogen abundance (N/O) is related to the oxygen abundance (O/H) in a manner that accounts for secondary production of nitrogen, largely following the updated prescription of Groves et al. (2004) in Gutkin et al. (2016). Depletion of metals onto dust grains is considered through definition of ξ_d, the dust-to-heavy element mass ratio parameter, following the treatment introduced in Charlot & Longhetti (2001). In the models described below, we initially assume $\xi_d = 0.3$, but we note that assuming different ξ_d values ($0.1 - 0.5$) does not impact the model N V/C IV and N V/He II ratios significantly (e.g., Mignoli et al. 2019).

We show the N V/C IV and N V/He II line ratios for our fiducial set of narrow line AGN models in Figure 8. The ionization parameter is varied between $\log U_S = -5$ and -1, and the metallicity is varied between $Z = 0.006\ Z_\odot$ and $4\ Z_\odot$. The N V/C IV and N V/He II ratios will be sensitive to the ionization parameter and the hardness of ionizing radiation given the relative ionization energies of each species (77, 54, and 48 eV for N V, He II, and C IV). We show how the line ratios increase with ionization parameter in the right panel of Figure 8. We see that N V can be as strong as He II and as strong as C IV for models with ionization parameters above $\log U_S = -2.5$. At a given ionization parameter, the highest N V/C IV and N V/He II ratios are reached for the highest metallicity models (see also Feltre et al. 2016). This is largely due to the adopted scaling between N/O and O/H. Even at the highest metallicities in this fiducial grid, none of the models approach the observed limits we place on the N V/C IV and N V/He II line ratios in CEERS-1025 and CEERS-7902 in Section 3.

Larger N V/He II and N V/C IV ratios can be obtained if the nitrogen abundance is enhanced relative to the Groves et al. (2004) relation. We explore the line ratios using a grid of models with two N/O values ($\log(\mathrm{N/O}) = 0$ and 0.7), each of which is held fixed as a function of O/H. At low metallicity, these N/O values represent significant nitrogen enhancements with respect to our fiducial models, as has been seen in a subset of *JWST*-detected galaxies. We consider mod-

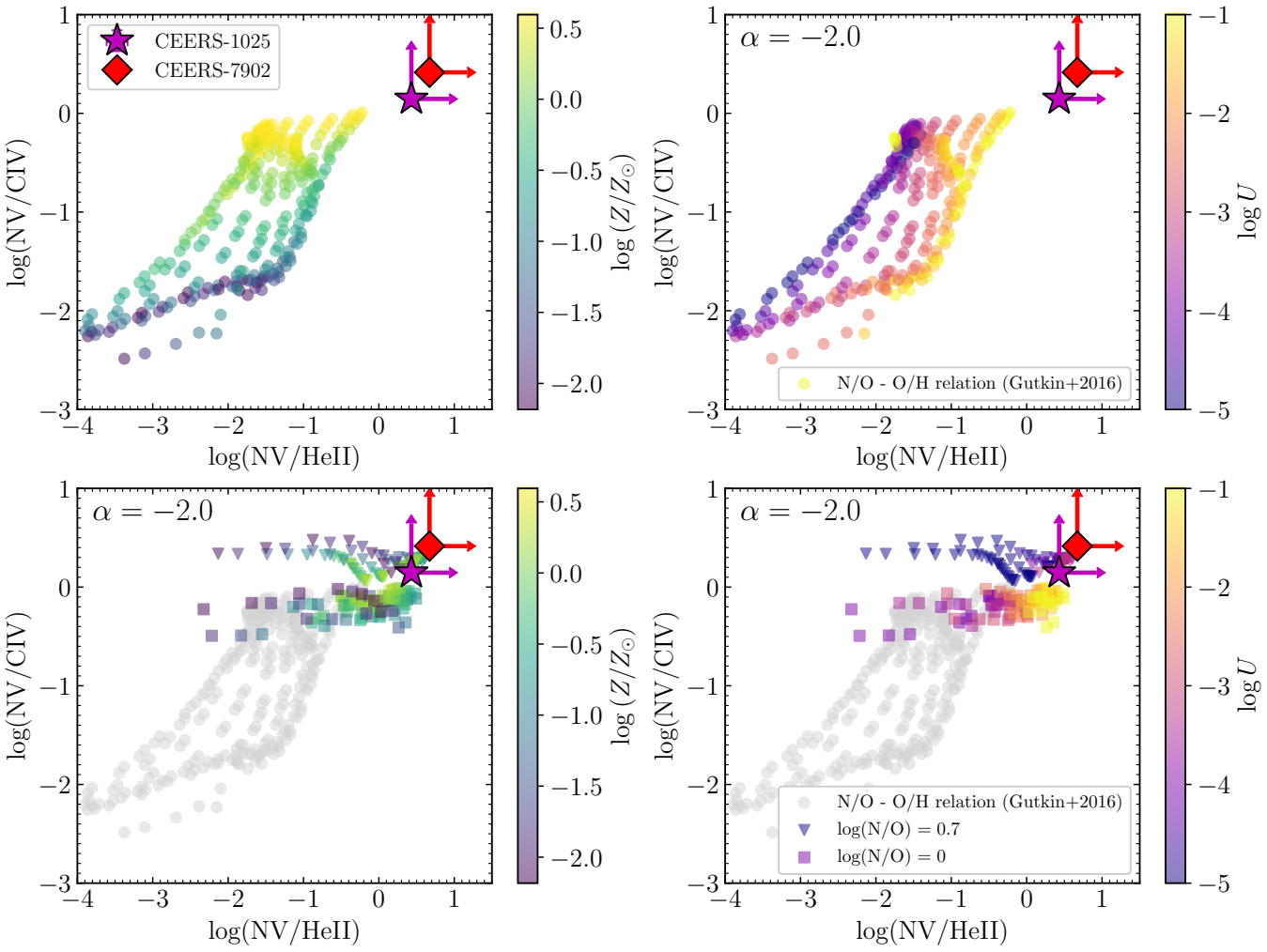

Figure 8. N V/C IV versus N V/He II line ratios of the two N V emitters CEERS-1025 (purple star) and CEERS-7902 (red diamond) and line ratios expected from photoionization models of narrow line AGN. The emitted spectrum of AGN accretion disk is assumed to be a power law $f_\nu \propto \nu^\alpha$ between $\lambda = 0.001$ μm to $\lambda = 0.25$ μm with $\alpha = -2.0$. The left two panels show models with different metallicity ($\log(Z/Z_\odot) = -2.2$ to 0.6) and the right two panels show models with different ionization parameters ($\log U = -5.0$ to -1.0). Models assuming N/O increasing with O/H following the prescription of Gutkin et al. (2016) are shown as circles. Models assuming fixed N/O are shown as upside-down triangles ($\log(\mathrm{N/O}) = 0.7$) and squares ($\log(\mathrm{N/O}) = 0$).

els with the same range of metallicity and ionization parameter as above. With the nitrogen-enhanced abundance pattern, the observed line ratios are significantly increased, particularly at low metallicities. We find that models with $\log(\mathrm{N/O}) = 0.7$ are able to reproduce the observed limits at a range of ionization parameters and metallicities that are either among the lowest or among the highest in the grid.

We note that these models also significantly boost the strength of N IV] emission, which we do not detect. One potential explanation for the absence of N IV] emission in nitrogen-enhanced clouds could be that the density is above the critical density for N IV] ($\sim 5 \times 10^9$ cm^{-3} for N IV] λ1486 and $\sim 1 \times 10^6$ cm^{-3} for [N IV] λ1483). This would imply the N V-emitting clouds are distinct from those seen in the rest of the narrow line spectrum, with densities similar to those expected from the broad line region. In this picture, it is conceivable that the N V emission stems from broad line region gas that is ejected in an outflow primarily along the polar axis, perpendicular to the line of sight (see Section 5). This would enable the line emission to probe gas with small line-of-sight dispersion, producing a narrow emission line. If the N V-emitting gas approaches BLR densities, then it may also contribute to the weakness of He II emission as collisional de-excitation becomes important at such large densities (e.g., Netzer et al. 1985; Mignoli et al. 2019).

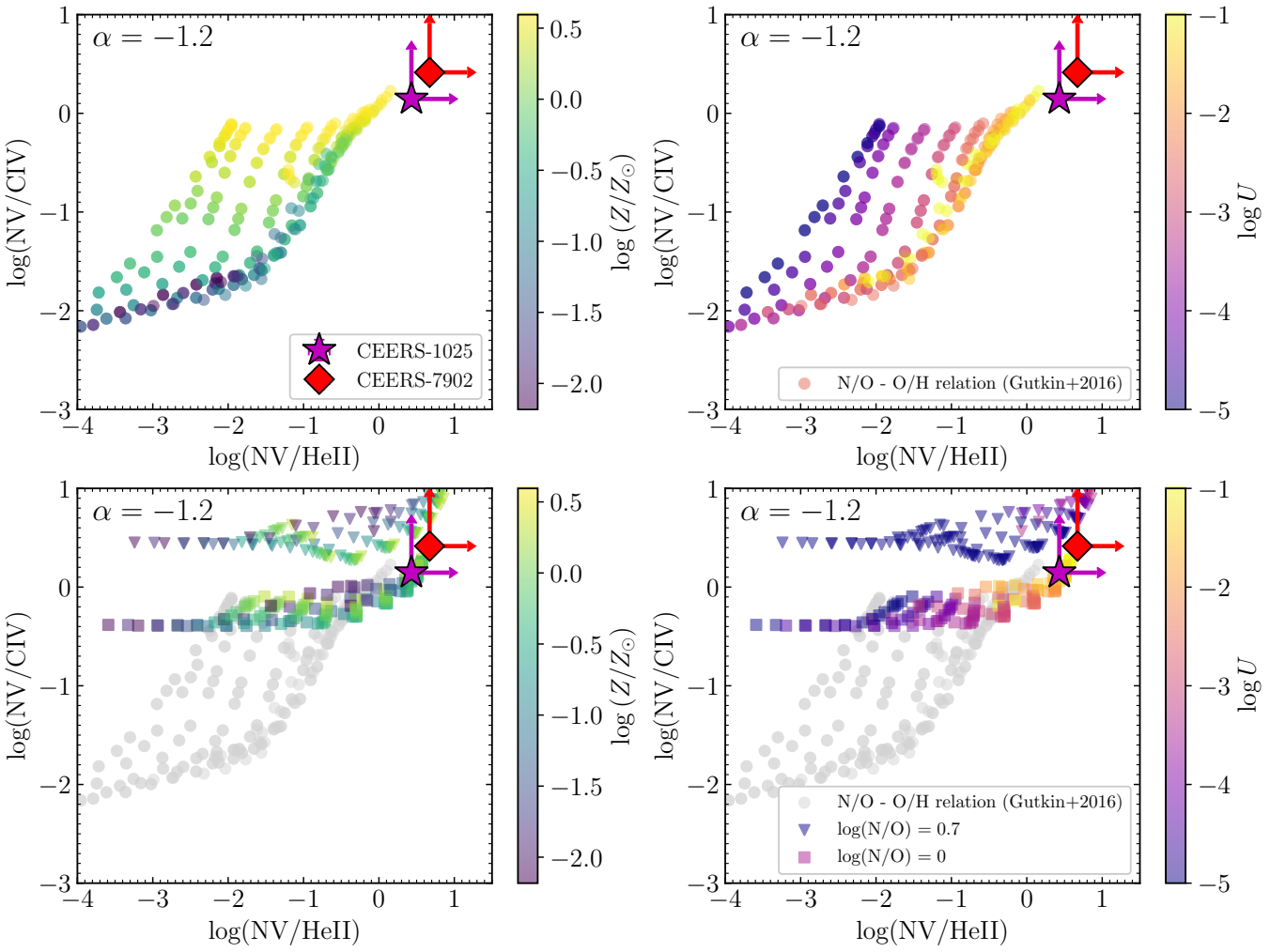

Figure 9. N V/C IV versus N V/He II line ratios of CEERS-1025 (purple star) and CEERS-7902 (red diamond), and line ratios expected from photoionization models with AGN accretion disk power law spectrum $\alpha = -1.2$. Symbols are shown in the same way as Figure 8.

There are several other factors which may boost the N V/He II and N V/C IV ratios. Given that N V requires the highest ionization energy of the three emission lines, a shallower AGN power law spectrum will boost N V relative to C IV and He II (see also Feltre et al. 2016). In Figure 9, we present models computed assuming an AGN spectrum with a shallower power law ($\alpha = -1.2$). The harder spectrum will both increase the electron temperature and present more photons capable of producing NV ions. We show the same four panels as in Figure 8, with N/O increasing with O/H (top panels) and two values of enhanced N/O (bottom panels). As expected, the N V/He II and N V/C IV ratios increase given the enhanced supply of 77 eV photons. We find that the median N V/He II ratio increases by 0.15 dex when using the shallower power law in fiducial models with fixed inner radius. The nitrogen-enhanced models are best able to reproduce the line ratios, with the largest ionization parameters required to produce the N V/He II ratios.

The N V/He II and N V/C IV line ratios also depend on the turbulent velocity of the particles in the gas clouds responsible for the line emission. In the original Feltre et al. (2016) models, the turbulent velocity was set to 0 km s^{-1}. As the turbulent line width is increased, continuum fluorescence of the resonant lines will become more important, boosting both N V and C IV fluxes. The N V/He II line ratios are boosted by 0.4 dex on average, at fixed ionization parameter and metallicity.

To summarize, the observations of CEERS-1025 and CEERS-7902 appear to indicate elevated N V/He II and N V/C IV ratios. We have shown that these can be reproduced with some combination of large ionization parameter and nitrogen-enhanced gas. This may indicate that the stellar populations formed near the nu-

cleus have peculiar abundance patterns, perhaps from a top-heavy initial mass function (e.g., Bekki & Tsujimoto 2023; Kobayashi & Ferrara 2024). Alternatively, the nitrogen-enhancements could come from tidal disruption events (e.g., Kochanek 2016; Cameron et al. 2023a). The line ratios could plausibly also be boosted if the accretion disk continuum power law is shallow in the UV, or if there are significant turbulent motions in the N V-emitting clouds. The detection of C III] and not C IV in CEERS-7902 may point to the presence of a significant contribution from a softer spectrum, potentially from massive stars in the host galaxy. Future investigations may also consider density-bounded models. If the radiation field is very hard, the N V-emitting gas may have its carbon in a higher ionization state (i.e., C^{4+}), and if the clouds are density-bounded we may primarily see N V and C V transitions, explaining the elevated N V/C IV emission. In this picture, the lower ionization state gas may again come from different regions in the galaxy.

While the models described above can explain the constraints on N V/He II and N V/C IV, they do not provide a natural explanation for the N V doublet ratios in both sources. One effect that may alter the N V line ratios is resonant scattering of (redshifted) Lyα and continuum photons by N V ions (e.g., Surdej & Hutsemekers 1987; Turnshek et al. 1988; Weymann et al. 1991; Hamann & Ferland 1993; Krolik & Voit 1998; Wang et al. 2010). The separation between Lyα and N V is ~ 5700 km s^{-1}. If there is a fast outflow of dense ionized gas surrounding the broad emission line region, it is possible that both Lyα and continuum will be redshifted into the N V resonance of ions in the outflow, producing N V line emission. Other resonant transitions (i.e., C IV) could also be excited by scattering in the broad absorption line region, but the presence of Lyα blueward of N V will act to boost N V relative to C IV. Resonant scattering is thus an attractive explanation for observations of large N V/C IV and N V/He II ratios.

Whether resonant scattering enhances N V in quasars remains debated. Hamann & Korista (1996) argue that scattering is unlikely to play a significant role in boosting N V emission since only a small fraction of Lyα photons would be scattered by gas in the broad absorption line region. However, Wang et al. (2010) have shown that N V can be enhanced by $2-3\times$ with realistic models of the geometry and optical depth profile in the broad absorption line (BAL) outflows. In their analysis, the impact of scattering on N V emission depends on the covering factor, optical depth, and velocity profile of the outflowing gas, and the intrinsic EW of Lyα. The outflow is assumed to be equatorial, providing a very large radial optical depth to Lyα photons. The scattered N V photons are more likely to escape tangentially, which results in both a narrower line profile and viewing-angle-dependent N V EW.

It is also possible that such a scattering scenario may alter the N V doublet ratio, but it requires some fine tuning. If the outflowing gas has maximum velocity between 5700 and 6700 km s^{-1}, redshifted Lyα will be more likely to excite the N V λ1239 transition than the N V λ1243 transition (here ignoring the width of Lyα). This will increase the N V λ1239 / N V λ1243 doublet ratio, potentially reaching values seen in CEERS-7902. However, the N V emission in CEERS-7902 does not appear significantly offset from systemic, making it difficult to understand in this framework unless the outflow is not only finely-tuned in its velocity profile but also oriented perpendicular to the line-of-sight. While detailed modeling may find a combination of geometries and optical depth and velocity outflow profiles which can explain the observations, such an analysis is currently beyond the scope of this paper. Knowledge of the kinematics of the ionized gas in the JWST-discovered AGN population is critical for interpreting resonant lines in the observed rest-frame UV spectra.

4. HOW COMMON ARE VERY HIGH IONIZATION LINES IN *JWST* SPECTROSCOPY AT $z > 4$?

In previous sections, we have described two galaxies with likely detections of N V identified in the GO 4287 program. In this section, we aim to place galaxies with very high ionization emission lines in a broader context, characterizing how commonly these galaxies appear in $z \gtrsim 4$ samples and comparing their properties to that of the full galaxy population. To achieve this goal, we assemble a large database of galaxies at $z > 4$ with publicly-available NIRSpec spectra and constrain the strengths of [N V], [Ne IV], and [Ne V] emission lines. We also identify the strongest He II emitters, noting that many of these are fully consistent with being stellar in origin. We choose these lines as they are most likely to be signposts of AGN photoionization (probing photons above the He^+ ionizing edge), although we note they are also plausibly powered by shocks. This complements several recent investigations of Type II AGN fractions (Scholtz et al. 2023; Mazzolari et al. 2024a), although we note our approach focuses only on the subset with high ionization emission lines. We describe the database in Section 4.1. We then discuss the demographics of galaxies with high ionization lines in Section 4.2. We both consider the presence of these lines in the full spectroscopic sample, as well as that in the subset of our sample

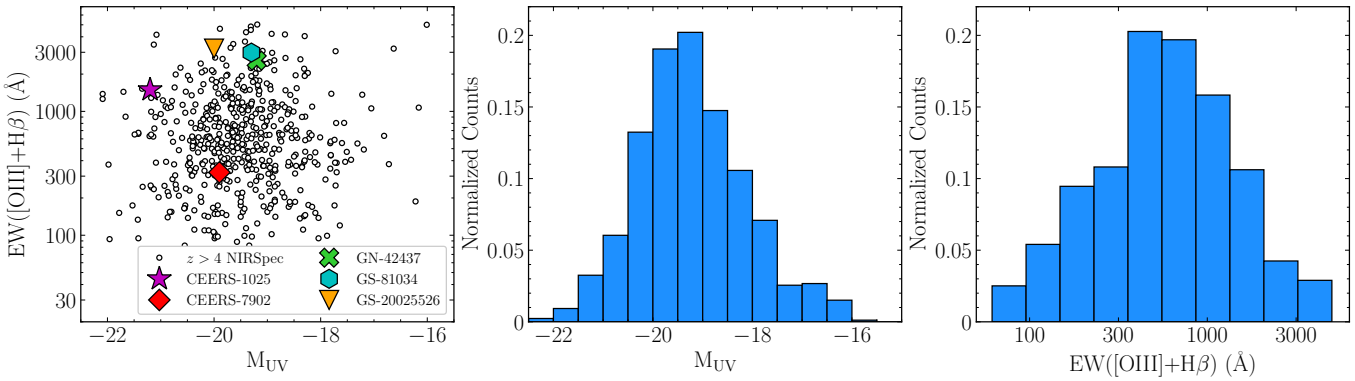

Figure 10. Left panel: M_{UV} versus [O III]+Hβ EW for galaxies at $z > 4$ with $R = 1000$ or $R = 2700$ NIRSpec grating spectra (black circles). We overplot objects with high ionization line detections: CEERS-1025 (N V λ1243, magenta star), CEERS-7902 (N V λ1239, red diamond), GS-20025526 (orange upside down triangle), GN-42437 (green cross; see also Chisholm et al. 2024), GS-81034 (cyan hexagon). Middle and right panels: M_{UV} and [O III]+Hβ EW distributions of $z > 4$ galaxies.

that are confirmed as broad line AGN with SEDs consistent with the LRD population.

4.1. *Public JWST/NIRSpec Spectra*

We construct a spectroscopic sample of $z > 4$ galaxies using NIRSpec spectra obtained from the following public observations: the JWST Advanced Deep Extragalactic Survey[3] (JADES, GTO 1180, 1181, PI: D. Eisenstein, GTO 1210, 1286, PI: N. Lützgendorf, GTO 1287, PI: K. Isaak, GO 3215, PIs: D. Eisenstein & R. Maiolino; Eisenstein et al. 2023a,b; Bunker et al. 2024; D'Eugenio et al. 2025), the GLASS-JWST Early Release Science Program[4] (GLASS, ERS 1324, PI: T. Treu; Treu et al. 2022), CEERS, GO 1871 (PI: J. Chisholm; Chisholm et al. 2024), and GO 2478 (PI: D. Stark; Topping et al. 2024a, 2025a) programs. All the NIRSpec observations were performed with the multi-object spectroscopy mode. The spectra were reduced following the same approaches described in Topping et al. (2025a) and Section 2. We refer readers to Tang et al. (2024) and Topping et al. (2025a) for a full description of the sample selection and analysis of the spectra of the public spectroscopic sample.

We briefly summarize the NIRSpec observations used in this section. Medium-resolution ($R = 1000$) NIRSpec grating spectra were taken in the JADES, CEERS, and GO 4287 programs. The exposure time of $R = 1000$ grating spectra spans from 0.9 hour to 11.7 hours (median 2.6 hours) for G140M, 0.9 hour to 6.9 hours (median 2.6 hours) for G235M, and 0.9 hour to 46.7 hours (median 2.6 hours) for G395M. For a galaxy with $H = 27$ at $z = 6$, this median depth results in a typical 3σ rest-frame EW limit of 18, 17, and 28 Å for G140M, G235M, and G395M spectra, respectively. While this is sufficient for rest-frame optical spectroscopy, we will show in Section 4.2.2 that this depth limits the constraints that can be placed on the weaker rest-frame UV emission lines. High-resolution ($R = 2700$) grating spectra were taken in the GLASS and GO 1871 programs, and JADES programs 1210, 1181, 1286, 1287 took G395H/F290LP spectra as well. For the small subset of our sample with $R = 2700$ spectra, the exposure time is 4.9 hours for G140H, $4.9 - 14.7$ hours (median 4.9 hours) for G235H, and $2.6 - 6.9$ hours (median 4.9 hours) for G395H. The typical 3σ EW limit (for a $H = 27$ galaxy at $z = 6$) reaches to 3, 4, and 15 Å for G140H, G235H, and G395H spectra, respectively. These limits are more conducive to rest-frame UV emission line detections, but we will show in the next subsection that the number of spectra approaching these limits is still small.

We assemble a spectroscopic database of $z \gtrsim 4$ galaxies from the aforementioned programs. In order to identify high ionization emission lines, we focus on galaxies with precise redshift measurements using strong emission line detections. Most of the sources have strong rest-frame optical emission lines (e.g., Hβ, [O III], Hα) in NIRSpec spectra ($z \lesssim 9.5$). For each of these objects, we simultaneously fit the available strong optical lines with Gaussian profiles, and compute the systemic redshift using the fitted line centers. For a small number of galaxies at $z \gtrsim 9.5$ where strong optical lines are shifted out of NIRSpec spectra, we determine the redshifts using other emission lines in the spectra (e.g., [Ne III], [O II], C III]). We do not identify objects purely based on the Lyα break in this database given the need for precise redshifts.

[3] https://jades-survey.github.io/

[4] https://archive.stsci.edu/hlsp/glass-jwst

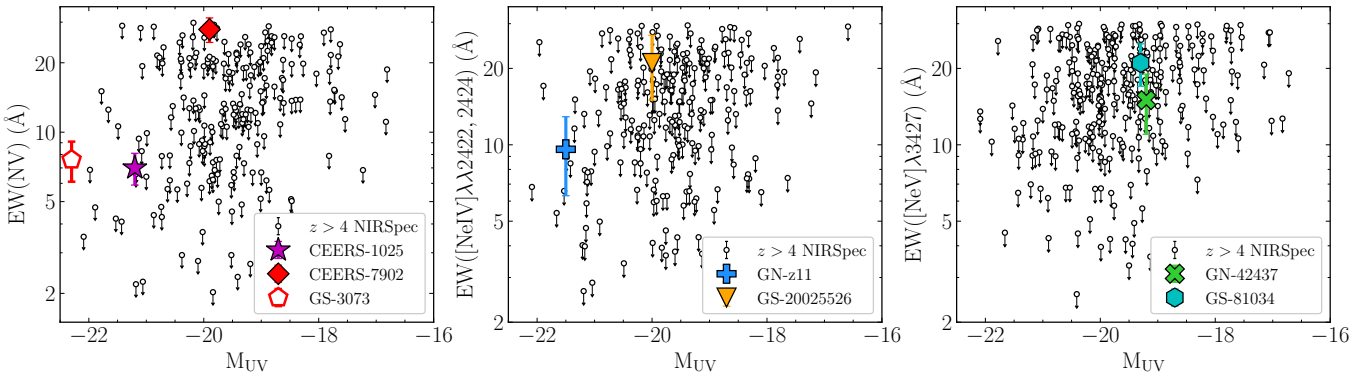

Figure 11. N V, [Ne IV] $\lambda\lambda 2422, 2424$, and [Ne V] $\lambda 3427$ EW versus M_{UV} for $z > 4$ galaxies with $R = 1000$ or $R = 2700$ NIRSpec grating spectra. We show sources with EW or 3σ EW limit < 30 Å (open black circles). For N V (left), EW measurements of single component are presented. For [Ne IV] (middle), we show the doublet EWs. Sources with high ionization line detections are overplotted with the same symbols in Figure 10 in addition with GN-z11 (blue plux; see also Maiolino et al. 2024b). We also overplot the $z = 5.55$ AGN GS-3073 (open red pentagon) with N V doublet EW $= 7.6 \pm 1.5$ Å (Ji et al. 2024).

To ensure robust constraints on high ionization emission lines, we limit our study to a sample of galaxies with NIRSpec medium- or high-resolution ($R = 1000$ or $R = 2700$) grating spectra (see Section 1). From the above programs we identify 846 such galaxies at $z > 4$ with NIRSpec $R = 1000$ or $R = 2700$ grating spectra. In addition, we include the new $z > 4$ galaxies identified from GO 4287 (Section 2). Because 5 of the 58 $z > 4$ galaxies in GO 4287 have been observed in CEERS before, this adds 53 new sources. Overall these form a sample of 899 galaxies with NIRSpec $R = 1000$ or $R = 2700$ spectra at $4.0 < z < 14.3$. We measure the emission line fluxes and EWs following the same procedures described in Section 2 and in Tang et al. (2024).

We show the absolute UV magnitudes and [O III]+Hβ EWs of the 899 galaxies in the spectroscopic sample in Figure 10. The M_{UV} are derived using the NIRCam photometry released by the DAWN JWST archive[5] team (Valentino et al. 2023). For the 899 galaxies in the $z > 4$ sample, the M_{UV} range from -22.1 to -15.9 with a median value of -19.3. The [O III]+Hβ EWs of galaxies at $z > 4$ span from 62 Å to 5027 Å, with a median value of 691 Å. This median [O III]+Hβ EW is comparable to the average EW of photometrically-selected galaxies at high redshift at fixed M_{UV} (Endsley et al. 2024).

We search for galaxies displaying N V, [Ne IV], He II, or [Ne V] emission lines in the $z > 4$ spectroscopic sample by visually inspecting their 2D spectra. There are 851 objects with NIRSpec $R = 1000$ or $R = 2700$ grating spectra covering at least one of these high ionization lines. We require S/N > 3 for a line detection. For the non-resonant lines ([Ne IV], He II, or [Ne V]), we require candidate detections to lie at wavelengths within 1 instrument resolution element offset from the line center defined by the redshift of the other narrow lines (± 300 km s^{-1} for $R = 1000$, or ± 111 km s^{-1} for $R = 2700$). For N V emission, we allow a larger velocity offset range (± 1000 km s^{-1}) given its resonant nature. We do not consider C IV in this paper, as a similar search has recently been presented in Topping et al. (2025a).

We first focus on N V, [Ne IV], and [Ne V]. We do find a very small number of galaxies that show plausible detections. Aside from the two likely N V lines presented in Section 3, the most clear example of a robust high ionization line detection in our database is GN-42437, the [Ne V] emitter at $z = 5.587$ presented in Chisholm et al. (2024). In our reduction, the [Ne V] line is detected at S/N=4 with a modest EW (EW $= 15 \pm 4$ Å), similar to what was reported in Chisholm et al. (2024). We also tentatively detect the [Ne IV] $\lambda 2422, 2424$ emission in GN-z11 ($z = 10.604$, EW $= 9.6 \pm 3.3$ Å) that was first reported in Maiolino et al. (2024b). The S/N of the line is low (3), but we consider this a plausible high ionization emission feature. The origin ofthe line emission in GN-z11 remains debated (e.g., Bunker et al. 2023; Maiolino et al. 2024b; Álvarez-Márquez et al. 2025). Whether the low S/N [Ne IV] detection reflects AGN activity or is consistent with a combination of shocks and massive stars is not yet clear. In addition to these sources, we find two new lower significance (S/N $= 3-3.5$) potential detections of [Ne IV] or [Ne V] emission. We consider these as very tentative, and note that deeper data will ultimately be required to verify whether or not the emission lines are real. One of the putative sources is GS-81034 ($z = 5.390$), where we find a potential emission feature (S/N $= 3$) near [Ne V] $\lambda 3427$ (EW $= 15 \pm 5$ Å). The other source is GS-20025526 ($z = 7.951$) where we

[5] https://dawn-cph.github.io/dja/index.html

note the presence of a low significance (S/N = 3.5) emission feature (EW = 21±6 Å) near the expected location of [Ne IV] $\lambda\lambda$2422, 2424. We verify that each of these two tentative detections is also detected in two independent reductions that are publicly available (DJA; de Graaff et al. 2024; Heintz et al. 2024, and JADES; Bunker et al. 2024; D'Eugenio et al. 2025). We summarize our measurements of the four sources with plausible high ionization line emission in Appendix A. Together with the two N V emitting galaxies identified in GO 4287 (Section 3), these sources form a small subset of galaxies with either confirmed or potential high ionization lines in archival NIRSpec medium- or high-resolution spectra at $z > 4$.

There are six sources at $z > 4$ (GS-9422, GS-58975, GS-202208, RXCJ2248-ID, A1703-zd2, and A1703-zd6) with detectable He II emission, all previously reported in the literature (Scholtz et al. 2023; Cameron et al. 2024; Curti et al. 2024; Topping et al. 2024a,b). We measure He II EW = 2 − 10 Å in our reductions of these spectra, consistent with what has been presented in previous investigations of the sources. Each of the grating spectra also show O III] $\lambda\lambda$1661, 1666 emission lines, allowing calculation of the O III]/He II flux ratios. The measured ratios (= 1.0 − 4.5) are consistent with expectations for stellar photoionization (Feltre et al. 2016). While we cannot rule out AGN activity, it seems likely that there is significant stellar contribution to the ionizing spectrum. In the following subsection, we will primarily focus on what the detections of N V, [Ne IV], and [Ne V] (816 objects with NIRSpec spectra covering at least one of these lines) suggest for the prevalence of very hard radiation fields at $z \gtrsim 4$.

The vast majority (810) galaxies do not show the high ionization emission lines described above in their NIRSpec spectra. But not all non-detections are equally constraining given the widely varying continuum strengths and sensitivity limits. We place 3σ upper limits on the EW of high ionization lines in the 810 galaxies without detections. There are 383, 476, and 632 galaxies with NIRSpec spectra covering N V, [Ne IV], and [Ne V], respectively. We derive the 25th-50th-75th percentiles of 3σ upper limits of N V (each single component of the doublet) EW = 11, 21, and 48 Å. For [Ne IV] ([Ne V]) line, the 25th-50th-75th percentiles of 3σ EW upper limit are 12, 21, and 43 Å (17, 32, and 60 Å), respectively. It is clear that many of the existing spectra are only able to detect very strong high ionization line emission, but there is a subset which allow useful constraints on the incidence of hard radiation fields.

4.2. *Fraction of Galaxies with High Ionization Lines*

In this subsection, we aim to quantify the fraction of $z > 4$ galaxies showing very high ionization emission lines in existing spectra. By focusing on lines above the He^+-ionizing edge, we aim to constrain the incidence of non-stellar photoionization in existing spectroscopic samples. As motivated in the previous subsection, we will focus on N V, [Ne IV], and [Ne V] detections. We first discuss the general population at $z > 4$ in Section 4.2.1 and then consider the subset of LRDs with confirmed broad lines in Section 4.2.2.

4.2.1. *The General Population at $z \gtrsim 4$*

As described in Section 4.1, many of the 816 galaxies in our $z > 4$ database do have deep enough spectra to place a sensitive limit on the high ionization line EW ($\simeq$ 10 Å, Section 3; see also, e.g., Chisholm et al. 2024). In order to put robust constraints on the fraction of high ionization line emitters, we primarily focus on galaxies with 3σ EW limit $<$ 10 Å for at least one of the high ionization lines. This limits us to a sample of 185 galaxies at $z > 4$. Among this subset, there are 87, 97, and 57 objects with deep enough spectra to reach N V, [Ne IV], or [Ne V] EW limits of $<$ 10 Å, respectively.

Using this database, we can compute the detection rate of each individual high ionization line. For the 87 sources with 3σ N V EW upper limits below 10 Å, two present N V emission (CEERS-1025 and CEERS-7902). This indicates that the fraction of galaxies with strong N V emission is fairly small ($2/87 = 2.3^{+3.0}_{-1.5}\%$; uncertainties estimated using the statistics for small numbers of events; Gehrels 1986). The percentage of galaxies presenting [Ne IV] ([Ne V]) emission line is $1/97 = 1.0^{+2.4}_{-0.9}\%$ ($1/57 = 1.8^{+4.1}_{-1.5}\%$). This increases to $2/97 = 2.1^{+2.7}_{-1.3}\%$ ($2/57 = 3.5^{+4.5}_{-2.3}\%$) for both lines if we include the tentative detections described above. If we consider a slightly larger EW threshold ($<$ 15 Å at 3σ), the fraction of high ionization line emitters decreases to $4/308 = 1.3^{+1.0}_{-0.6}\%$ ($6/308 = 1.9^{+1.2}_{-0.8}\%$ if including tentative detections). These results suggest that strong very high ionization lines appear rarely in $z \gtrsim 4$ galaxies, with only a few percent of the population exhibiting N V, He II, [Ne IV], or [Ne V] with EW $>$ 10 Å.

The fraction of high ionization line emitters is comparable if we limit our sample to galaxies in our spectroscopic database without known broad emission lines (i.e., removing broad line AGN). To quantify the fraction in this case, we remove the 19 broad line AGN (with Balmer emission line FWHM $>$ 1000 km s^{-1}) in our $z > 4$ sample. This leaves 166 galaxies with 3σ EW limit $<$ 10 Å for at least one of the N V, [Ne IV], or [Ne V] line. We find 5 plausible high ionization lines in this sample, resulting a fraction of $3.0^{+2.0}_{-1.3}\%$. This fraction

is somewhat lower than that reported in several recent studies (Scholtz et al. 2023; Mazzolari et al. 2024a), but we note those investigations also included galaxies identified by rest-frame optical diagnostics. A deeper spectroscopic database will ultimately be required to better establish the fraction of high ionization lines and the viability of low S/N detections. But even with the existing database, it appears clear that very strong (EW $>$ 10 Å) high ionization lines probing above 54 eV are fairly rare in the overall galaxy population at $z \gtrsim 4$. We note that our high ionization line fraction is roughly comparable to that measured in ground-based spectra at $z \simeq 2-3$ (Hainline et al. 2011), however direct comparison to this value is difficult given the different magnitudes of the respective samples (the Hainline et al. 2011 sample is significantly brighter) and the different selection criteria that have been used for identifying high ionization detections. As a result, the relative AGN fractions may also reflect mass-dependent differences between the two samples.

4.2.2. *High Ionization Lines in LRDs*

To place the detection of N V in CEERS-7902 in context, we investigate how frequently strong high ionization emission in BL AGN in the $z > 4$ spectroscopic sample introduced in Section 4.1. We specifically focus on the subset of those that would be classified as LRDs, but we note that this represents a subset of the total BL AGN population (Hainline et al. 2025).

To assemble the sample of LRDs with deep grating rest-frame UV spectra, we apply the selection criteria similar to that applied in Matthee et al. (2024), requiring detection of broad Hβ or Hα emission (S/N $>$ 5) with FWHM $>$ 1000 km s^{-1}. Then we select red and compact sources from the BL AGN following the color criteria in Kokorev et al. (2024) and Labbe et al. (2025). For galaxies at $z < 6$, we apply color cuts of F115W $-$ F150W $<$ 0.8, F200W $-$ F277W $>$ 0.7, and F200W $-$ F356W $>$ 1.0. For galaxies at higher redshift ($z > 6$), we apply F150W $-$ F200W $<$ 0.8, F277W $-$ F356W $>$ 0.6, and F277W $-$ F444W $>$ 0.7. To ensure we select compact sources, we further require that the F444W images are spatially unresolved using the ratio of F444W flux densities measured between 0″.4 and 0″.2 apertures $f_{\rm F444W}(0''.4)/f_{\rm F444W}(0''.2) < 1.7$. With these selection criteria, we identify 18 LRD BL AGN among the 899 galaxies in our grating rest-frame UV database. We list the 18 LRDs at $z > 4$ with NIRSpec grating spectra in Table 3, whose NIRSpec spectra have also been presented in literature (Harikane et al. 2023; Kocevski et al. 2023, 2024; Maiolino et al. 2024a; Taylor et al. 2024; Wang et al. 2024b; Juodžbalis et al. 2025).

We characterize the strength of narrow rest-frame UV high ionization emission lines (N V, He II, [Ne IV], and [Ne V]) in the NIRSpec spectra of these 18 LRDs. The NIRSpec $R = 1000$ or $R = 2700$ grating spectra cover N V emission lines in 8 LRDs. Four of these eight LRDs have robust N V constraints with 3σ EW upper limit $<$ 10 Å, and we detect N V in one of them (CEERS-7902, see Section 3.2). There are 15 LRDs with NIRSpec grating spectra covering He II. No He II emission is seen in the seven LRDs with deep enough spectra to detect EW = 10 Å line emission. There are 13 and 16 LRDs with NIRSpec grating spectra covering [Ne IV] and [Ne V], respectively. Neither line is seen in this sample. The [Ne IV] and [Ne V] EW limits are relatively large, with only 3 LRDs with [Ne IV] EW limit $<$ 10 Å and 4 LRD with [Ne V] EW limit $<$ 10 Å. These results underscore how few grating spectra have yet reached depths necessary to detect high ionization lines at EW = 10 Å. Larger samples of deep $R = 1000$ spectra will soon allow improved constraints, but based on the presence of N V emission in the small existing sample, it is possible that high ionization lines may be relatively common in LRD spectra.

We also search for narrow C IV $\lambda\lambda$1548, 1551 emission. Fifteen of the galaxies have NIRSpec $R = 1000$ or $R = 2700$ grating spectra with wavelength ranges covering C IV. We detect unresolved C IV doublet emission in one LRD, GN-954 ($z = 6.7597$). This line was previously reported in the census of C IV emission presented in Topping et al. (2025a). We measure a C IV doublet EW = 31.5 $\pm$ 5.6 Å, consistent within 1σ of the EW reported in Topping et al. (2025a) (EW = $23.3^{+3.8}_{-3.7}$ Å). This on its own is not enough to verify the line is powered by AGN photoionization, but it is plausible that a non-stellar hard radiation field contributes given the broad lines detected in the rest-frame optical. For the remaining 14 LRDs with C IV constraints, we do not identify C IV emission, with 7 of them having 3σ EW upper limits $<$ 10 Å. While the statistics are poor, this suggests a C IV detection rate of $1/8 = 12.5^{+23.7}_{-10.4}$%.

Above we have focused on narrow rest-frame UV emission lines in LRDs. We can also constrain the presence of broad permitted UV lines in the spectra of the 18 LRDs in grating rest-frame UV coverage. Lambrides et al. (2024) have recently shown that no broad high ionization UV lines are present in a sample of 8 LRDs. We find the same result is present with our sample of 18 LRDs. Using the spectra, we can constrain the upper limits of luminosities of broad high ionization emission lines (N V, C IV, He II, [Ne IV], [Ne V]). To do so,

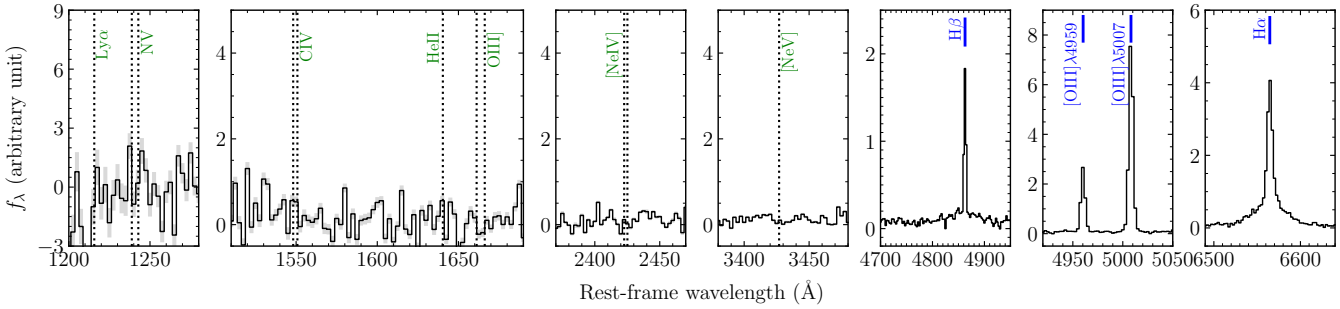

Figure 12. Composite NIRSpec grating spectrum of the 18 LRDs at $z > 4$. High ionization emission lines (N V, C IV, He II, [Ne IV], [Ne V]) are not detected, which are marked by green text. We show detections of narrow forbidden [O III] λ4959 and λ5007 lines, as well as Hβ and Hα emission line with narrow and broad components.

Table 3. LRDs confirmed as BL AGN with NIRSpec medium- and high-resolution grating sampling rest-frame UV.

ID	PID	R.A. (deg)	Decl. (deg)	$z_{\rm spec}$	$M_{\rm UV}$ (AB mag)	Line	$\rm FWHM_{broad}$ (km s^{-1})	References
CEERS-672	1345	214.889677	+52.832977	5.6669	−17.7	Hα	1394 ± 333	(1,3,7)
CEERS-746	1345	214.809142	+52.868484	5.6227	−18.3	Hα	1630 ± 177	(1,2,3,4,7)
CEERS-2782	1345	214.823453	+52.830281	5.2410	−20.0	Hα	2084 ± 305	(1,2,7)
CEERS-7902	4287	214.983038	+52.956205	6.9827	−19.9	Hβ	3394 ± 259	(3,4,8,this work)
CEERS-10444	4287	214.892231	+52.877651	6.6835	−19.9	Hβ	3816 ± 128	(3,4,7,8,this work)
GN-954	1181	189.151972	+62.259639	6.7597	−19.9	Hα	1839 ± 84	(5,9)
GN-1093	1181	189.179742	+62.224629	5.5946	−18.0	Hα	2046 ± 216	(5,9)
GN-11836	1181	189.220587	+62.263675	4.4087	−19.3	Hα	1472 ± 182	(5,9)
GN-20621	1181	189.122515	+62.292850	4.6814	−17.7	Hα	1900 ± 253	(5,9)
GN-53757	1181	189.269778	+62.194208	4.4475	−19.1	Hα	2044 ± 106	(5,9)
GN-61888	1181	189.168016	+62.217013	5.8738	−18.6	Hα	1528 ± 131	(5,9)
GN-73488	1181	189.197396	+62.177233	4.1327	−18.9	Hα	2225 ± 51	(5,9)
GS-9597	1180	53.166115	−27.772043	6.3057	−19.0	Hα	2565 ± 228	(4)
GS-9515	1210	53.132763	−27.801838	4.6487	−18.6	Hα	1598 ± 166	(5,9)
GS-13704	1210	53.126677	−27.818102	5.9198	−19.3	Hα	2288 ± 278	(3,4,5,9)
GS-38562	1286	53.135876	−27.871755	4.8222	−18.9	Hα	1909 ± 52	(9)
GS-172975	1286	53.087715	−27.871211	4.7421	−17.5	Hα	1538 ± 140	(3,4,9)
GS-204851	1286	53.138541	−27.790279	5.4825	−19.1	Hα	2010 ± 69	(6,9)

NOTE—Column "PID" shows the JWST program ID. Column "Line" lists the Balmer emission line with the highest S/N broad component identified in NIRSpec spectra, whose broad line widths are listed in column "$\rm FWHM_{broad}$". **References**: (1) Harikane et al. (2023); (2) Kocevski et al. (2023); (3) Kocevski et al. (2024); (4) Kokorev et al. (2024); (5) Maiolino et al. (2024a); (6) Matthee et al. (2024); (7) Taylor et al. (2024); (8) Wang et al. (2024b); (9) Juodžbalis et al. (2025).

we assume a broad line width that is the same as that measured from broad Balmer emission in the rest-frame optical (Table 3). Then for each high ionization line, we compute the 1σ upper limit by integrating the error spectrum in quadrature using a spectral window spanning $2\times$ $\rm FWHM_{broad}$. For the 18 LRDs, the median 3σ upper limits of the broad emission line luminosities are 2.6×10^{41} erg s^{-1} for N V, C IV, or He II, and 1.5×10^{41} erg s^{-1} for [Ne IV] and 1.1×10^{41} erg s^{-1} for [Ne V].

To place more stringent constraints on the broad high ionization emission lines, we create a composite spectrum of 18 LRDs. We first shift individual LRD spectra to the rest-frame using the systemic redshifts measured from narrow [O III] lines. Each spectrum is then interpolated to a common rest-frame wavelength scale of 2.5 Å

($R \simeq 500-1000$ at rest-frame UV) and normalized by its Hβ luminosity. Finally the spectra are median stacked and the composite spectrum is multiplied by the median Hβ luminosity of the 18 LRDs. The composite spectrum also does not show broad UV lines. To constrain the broad emission luminosities, we again assume a line width equal to the average broad Balmer emission line width (FWHM = 1950 km s^{-1}) and integrate the composite error spectrum in quadrature. The 3σ upper limits of broad line luminosities estimated from the composite spectrum are 4.4×10^{40} erg s^{-1} for C IV or He II, and 1.5×10^{40} erg s^{-1} for [Ne V]. The upper limits estimated from our composite LRD spectrum are consistent with the upper limits for systems presented in Lambrides et al. (2024).

Detailed modeling of the high ionization broad line luminosities is beyond the scope of this paper. However, Lambrides et al. (2024) have presented expected high ionization broad line luminosities expected for slim disk models with weak EUV radiation fields resulting from the effects of photon trapping. Based on their results, we may have expected to detect broad emission lines in the UV at the composite luminosity limit, even after accounting for potential dust extinction effects. This result may suggest that the intrinsic UV spectrum of LRDs is (on average) weak, as suggested in Lambrides et al. (2024). However, it appears plausible that some LRDs may indeed power hard radiation fields given the presence of narrow high ionization lines. And others may have broad UV lines strongly attenuated by H I scattering if there is complete line-of-sight coverage by dense hydrogen that is excited to the $n = 2$ level (e.g., Inayoshi & Maiolino 2025; Ji et al. 2025; Naidu et al. 2025). Such dense hydrogen would effectively scatter away UV photons from the disk and the broad line region. Deeper rest-frame UV spectra of individual LRDs should reveal whether a subset may show broad UV lines. Übler et al. (2023) present a spectrum of a $z = 5.55$ AGN with broad He II λ1640 emission exceeding the luminosity limit of our composite. As larger rest-frame UV spectroscopic databases emerge, it should be possible to determine whether the properties of broad line AGN with high ionization lines differ from those without.

5. DISCUSSION

We have quantified the presence of broad and narrow high ionization lines in a large sample $z \gtrsim 4$ *JWST* spectra. The visibility of high ionization UV lines will depend both on the intrinsic EUV radiation field and on the opacity provided by gas and dust. Our work supports earlier indications that high ionization UV lines are rare (Lambrides et al. 2024), both in LRDs and in the general population. However, we do detect narrow N V emission in two $z > 6$ galaxies, one of which is an LRD previously shown to have broad Hβ emission (Kocevski et al. 2024; Wang et al. 2024b), while the other shows only narrow lines in the rest-frame UV and optical. Neither shows broad UV emission lines. These narrow line detections add to a small but growing database of galaxies with high ionization lines (Treiber et al. 2024; Topping et al. 2025a; Labbe et al. 2025). This may indicate that at least a subset of the population does power intense EUV ionizing spectra. With these sources, we can begin to explore the conditions which facilitate the high ionization features.

In the case of the N V-emitting LRD presented in Section 3.2 (CEERS-7902), we observe a Balmer break and Hβ absorption. In the context of recent papers (Inayoshi & Maiolino 2025; Ji et al. 2025; Naidu et al. 2025; de Graaff et al. 2025), this indicates the presence of extremely dense neutral gas around the accretion disk in the N V emitter, with neutral hydrogen populating the $n = 2$ level. Naidu et al. (2025) suggest that the dense gas likely uniformly covers the disk and broad line region in the case of the LRD MoM-BH*-1. In that system, uniform neutral gas coverage is critical for powering the strong Balmer break ($f_{\nu,4050}/f_{\nu,3670} = 7.7^{+2.3}_{-1.4}$) and producing a symmetric Hβ absorption feature (c.f. Juodžbalis et al. 2025). A similar picture may also apply to The Cliff, another LRD with a very strong ($f_{\nu,4050}/f_{\nu,3670} = 6.9^{+2.8}_{-1.5}$) Balmer break (de Graaff et al. 2025).

The presence of narrow N V emission and Balmer series absorption in the spectrum of CEERS-7902 may indicate that its dense neutral gas (with hydrogen in its $n = 2$ level) does not uniformly cover its nucleus, allowing ionizing radiation to escape to the narrow line region. One possibility is that the ionizing radiation is collimated into a funnel-like geometry, with the opening angle directed along the rotation axis, as predicted for AGNs undergoing super-Eddington accretion (e.g., Sikora 1981; Madau 1988; Madau & Haardt 2024; Pacucci & Narayan 2024). It has recently been noted that the supercritical disk geometry and anisotropic radiation field may help explain the absence of X-rays in most LRDs (Pacucci & Narayan 2024; Madau 2025). This configuration may also be useful for understanding the narrow and broad line spectra (e.g., Wang et al. 2014). If our viewing angle is oriented far from the rotation axis (i.e., closer to edge-on), the ionization cone would be oriented closer to perpendicular to the line-of-sight. The AGN continuum would ionize gas clouds within the ionization cone at larger impact parameters. At these distances, the line-of-sight opacity to UV pho-

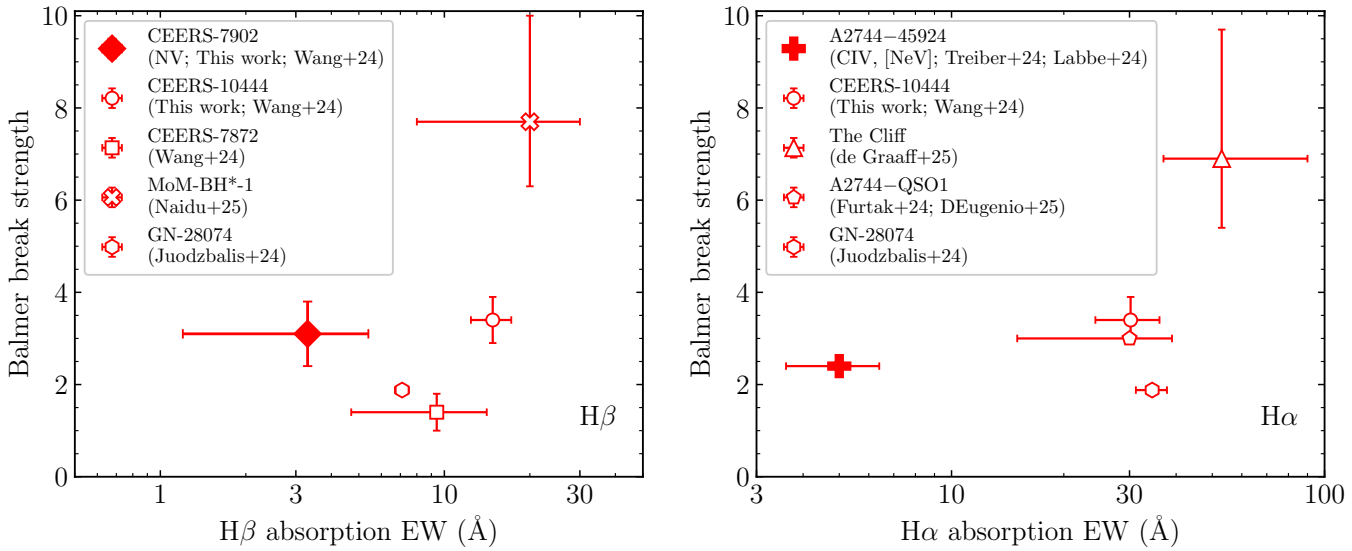

Figure 13. Balmer break strengths $f_{\nu,4050}/f_{\nu,3670}$ versus Balmer absorption line EWs of LRDs presented in this work and literature (Furtak et al. 2024; Juodžbalis et al. 2024; Labbe et al. 2024; Treiber et al. 2024; Wang et al. 2024b; de Graaff et al. 2025; D'Eugenio et al. 2025; Naidu et al. 2025). The left panel shows LRDs with Hβ absorption lines, and the right panel shows those with Hα absorption lines. The N V emitter CEERS-7902 is marked by solid red diamond, and the LRD with prism C IV and [Ne V] detections identified in Treiber et al. (2024) and Labbe et al. (2024) is marked by solid red cross.

tons is much lower. As a result, we should be able to observe narrow high ionization UV lines even if our line-of-sight to the central disk is significantly obscured by dense neutral gas, as in the case in CEERS-7902 (Figure 14). In this configuration, the broad UV lines would be significantly attenuated by absorption from hydrogen atoms in the $n = 2$ level, potentially explaining how we might see narrow high ionization line emission without seeing broad UV lines. Of course, the prominence of the narrow high ionization lines would be additionally boosted if the line-of-sight covering fraction of dense neutral gas is not uniform, allowing a larger volume of the narrow line region to be irradiated with the AGN spectrum. In practice, our ability to detect the narrow high ionization lines will further depend on the contribution from massive stars in the host galaxy, as significant underlying UV continuum emission would reduce the emission line EWs.

It is possible that the N V-emitting clouds are distinct from those producing the rest of the narrow line spectrum. This may help explain why CEERS-7902 presents N V and C III] without any hint of C IV emission. In this picture the C III] emission would come from a different region than the N V emission, possibly from clouds outside of the AGN ionization cone where the softer stellar ionizing spectrum dominates. In Section 3.4, we suggested that the observed N V/C IV and N V/He II ratios could be explained if the clouds were nitrogen-enhanced with densities similar to that of the broad line region, as this would help explain the absence of N IV] emission. One possibility is that the N V emission comes from broad line region gas that has been ejected in an outflow along the polar axis perpendicular to the line-of-sight, such that the majority of their motion is not in the line-of-sight. The high ionization clouds may be more centrally concentrated than those dominating line narrow line emission from lower ionization species.

We may also expect to see additional signatures of AGN photoionization in the narrow line spectra of LRDs with high ionization lines. As described in Section 3.2.2, the rest-frame optical spectrum of CEERS-7902 shows [O III]λ4363/Hγ vs. [Ne III]/[O II] ratios that are not expected in star formation galaxies (Mazzolari et al. 2024b), likely reflecting the enhanced heating provided by the AGN continuum on the narrow-line clouds. We also report a tentative detection of the low ionization line [O I] λ6302 in CEERS-7902 (and a clear detection in the LRD CEERS-10444), often seen in partially-ionized regions of AGNs. The implied [O I] λ6302/Hα ratio of CEERS-7902 is consistent with expectations for AGN photoionization (e.g., Kewley et al. 2001; Feltre et al. 2016; Mazzolari et al. 2024a). Given that we see both of these features alongside a strong Balmer break and Hβ absorption, we may again expect that a hard ionizing radiation field from the AGN is escaping to the narrow line region in spite of the indications of dense neutral gas absorption along the line-of-sight.

In the above discussion, we have assumed the high ionization lines are powered by AGN photoionization. However, the highly-ionized species may also originate

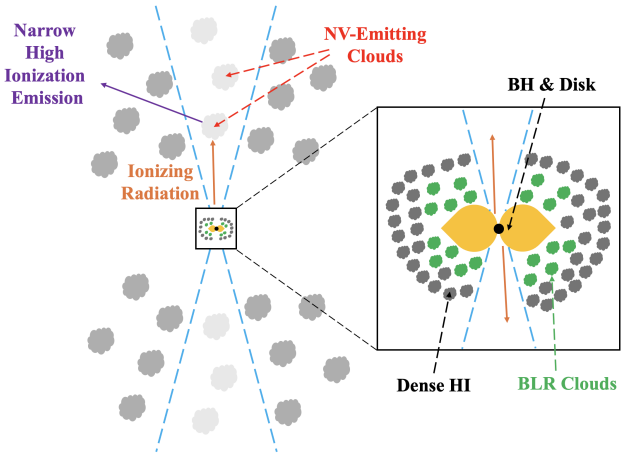

Figure 14. Schematic illustrating a scenario for AGN photoionization of narrow line clouds in LRDs with significant line-of-sight covering of extremely dense neutral hydrogen (dark grey) in the vicinity of the BLR clouds (green) and the disk (orange), resulting in Balmer series absorption in the rest-frame optical spectrum. If the line-of-sight covering fraction of dense gas and BLR clouds is large, the narrow line region may still be ionized along the polar axis, perpendicular to the line-of-sight. The narrow high ionization lines may be further amplified if the line-of-sight covering fraction of dense hydrogen and the BLR is reduced.

from other processes. Fast radiative shocks could create the conditions necessary to power the high ionization lines without requiring a hard EUV AGN spectrum (e.g., Allen et al. 2008; Izotov et al. 2012; Alarie & Drissen 2019). If turbulent velocities are as large as suggested in some recent investigations (e.g., Naidu et al. 2025), such shocks may not surprising. However, the UV line emission produced by the shocks would potentially be absorbed by the dense neutral gas implied by the Balmer break (with hydrogen predominantly in the $n = 2$ level) if the line-of-sight covering fraction is near-unity, unless there is significant line production in the outer optically thin regime. It is also possible that massive stars in the host galaxies contribute. While it is unlikely that normal stellar populations supply the photon budget responsible for producing species with ionization energies well above the He^+ ionizing edge (i.e., N V, [Ne V]), it is conceivable that the dense conditions in LRDs produce a population of ionizing sources unlike that seen at lower redshifts. Deeper spectra should enable these alternative possibilities to be tested in greater detail.

As larger samples of deep rest-frame UV spectra are obtained, it will be possible to compare the properties of LRDs exhibiting high ionization UV lines with those that do not. We may expect high ionization narrow lines to be less likely in LRDs with the disk and broad line region blanketed by dense H I gas (Inayoshi & Maiolino 2025). Perhaps surprisingly in that context, the existing database reveals that two of the LRDs with high ionization narrow line detections (CEERS-7902 and A2744-45924) do have Balmer breaks and Balmer series absorption features. However, as shown in Figure 13, these two LRDs have weaker Hβ or Hα absorption lines and lower amplitude Balmer Breaks than those recently presented in Naidu et al. (2025) and de Graaff et al. (2025). This may indicate that galaxies with high ionization lines have a lower line-of-sight covering fraction of extremely dense neutral gas. It may also point to a different intrinsic spectrum or a larger opening angle for the funnel geometry, both of which may relate to the accretion physics (e.g., Wang et al. 2014; Jiang et al. 2019). More detailed photoionization modeling jointly fitting the high ionization lines and the Balmer series absorption is beyond the scope of this paper, but should yield valuable insights as higher quality spectra are obtained in the future. If the geometry described above is valid, it should also be possible to identify AGNs viewed pole-on, along the funnel-like ionization cone. These sources should be much brighter in the UV, resulting in lower high ionization EWs (Madau 2025). If there are gas clouds experiencing fast outflows along the polar axis, we should similarly see evidence in the small subset of AGNs viewed closer to pole-on.

Of course, the broad line LRDs described above are only a subset of the $z \gtrsim 4$ AGN population (e.g., Hainline et al. 2025). Identification and characterization of low luminosity AGNs that do not show broad lines will help place the LRD and broad line AGN population in context. It is well known that traditional rest-frame optical narrow line diagnostics struggle in identifying Type II AGN at very high redshift owing to the low metallicity and extreme ionization gas conditions that become common in star forming galaxies (e.g., Masters et al. 2014; Coil et al. 2015; Scholtz et al. 2023; Übler et al. 2023; Mazzolari et al. 2024a). New diagnostics focused on high ionization or temperature-sensitive emission lines will help (e.g., Feltre et al. 2016; Mazzolari et al. 2024b), but if the UV radiation field of AGNs is intrinsically weak or ionizing photons are strongly attenuated prior to reaching the narrow line region, these diagnostics will also be incomplete.

Progress requires continued efforts to identify Type II AGN as *JWST* spectroscopic samples grow in number. We have presented an N V emitter at $z = 8.7$ without broad lines in its rest-frame optical spectrum. This galaxy has a large [O III]+Hβ EW (1682 Å) and a very blue continuum slope ($\beta = -2.5$), comparable to other systems dominated by very young stellar populations at

similar redshifts. This galaxy is one of a small sample of Type II AGN candidates at $z \gtrsim 4$ discovered with *JWST* spectroscopy (Scholtz et al. 2023; Übler et al. 2023; Mazzolari et al. 2024a; Chisholm et al. 2024; Silcock et al. 2024). Our investigation of 851 public NIRSpec grating spectra suggests that the fraction of $z \gtrsim 4$ galaxies with high ionization lines (N V, He II, [Ne IV], [Ne V]) is $2.2^{+1.7}_{-1.0}$%, where here this census refers only to lines with EW > 10 Å. This percentage is broadly similar to that measured in ground-based follow-up of UV-selected galaxies at $z \simeq 2-3$ (e.g., Hainline et al. 2011). We emphasize that this number should be considered as merely the fraction of galaxies with very high ionization lines and not as an AGN fraction. Deeper spectra will be required to validate low S/N detections and isolate the most likely powering mechanism (i.e., shocks, AGN).

Our results suggest that a subset of $z > 4$ AGN may have elevated nitrogen emission line strengths, with detectable N V in cases where C IV and He II are not present. While the precise physics driving the strength of the N V emission is not clear, it is possible that a nitrogen enhanced abundance pattern may be partially responsible (see Section 3.4), as has been seen in other AGN with *JWST* (e.g., Ji et al. 2024; Napolitano et al. 2024; Tripodi et al. 2024; Isobe et al. 2025). This may suggest that the star formation conditions near the nucleus produce unusual abundance patterns, perhaps reflecting a very top heavy initial mass function capable of producing nitrogen-enhancements (e.g., Bekki & Tsujimoto 2023; Kobayashi & Ferrara 2024). Alternatively we may be seeing the effects of gas produced via tidal disruption events (e.g., Kochanek 2016; Cameron et al. 2023a). One of the key questions is whether this is a common phase in the JWST-detected AGN population. The frequency of the high ionization lines will depend on the radiation field, the gas covering fraction and kinematics, and the strength of the underlying UV continuum. To-date only four LRDs have been observed with NIRSpec grating spectroscopy capable of detecting N V at EW > 10 Å. For reference, the composite of Type II AGN in Hainline et al. (2011) has N V EW = 5.6 Å. Deeper spectra sensitive to narrow N V emission with EW > 5 Å (in both the general population and in the LRDs) may uncover a larger sample of AGNs with hard radiation fields and (potentially) nitrogen-enhanced gas conditions.

6. SUMMARY

We present a search for very high ionization emission lines (N V, [Ne IV], [Ne V]) in 851 galaxies at $z > 4$ with *JWST*/NIRSpec medium- or high-resolution ($R = 1000$ or $R = 2700$) grating spectra. The dataset includes new $R = 2700$ G140H/F100LP spectra of 58 sources in the EGS field observed through the GO 4287 program. From the new observations we identify two likely narrow N V emission line detections, providing indications of hard radiation fields usually associated with AGNs. We summarize our findings below.

1. We detect narrow N V λ1243 emission (EW = 7.0 ± 1.1 Å) in the new G140H spectrum of CEERS-1025 ($z = 8.7166$), a galaxy previously-confirmed via rest-frame optical emission lines in the CEERS program (Nakajima et al. 2023; Tang et al. 2023). The rest-frame optical spectrum reveals no broad lines, and the SED is similar to that seen in star forming galaxies dominated by young stellar populations. No C IV or He II emission is seen in the rest-frame UV spectrum of CEERS-1025.

2. We report rest-frame UV spectroscopy of two LRDs, both previously confirmed to show broad hydrogen emission lines and Balmer series absorption, as expected for broad line AGN surrounded by extremely dense neutral gas with hydrogen populating its $n = 2$ level. The rest-frame UV spectrum of one of the two LRDs (CEERS-7902, $z = 6.9827$) shows strong, narrow N V λ1239 (EW = 27.9 ± 3.4 Å) and C III], but C IV and He II are not detected. The other LRD (CEERS-10444 at $z = 6.6836$) also shows C III], but N V is not covered in the G140H spectrum, and C IV and He II are not detected. In spite of the indications of dense neutral gas absorption around the central disk and broad line region, both LRDs show the potential influence of AGN photoionization on the narrow emission lines (i.e., [O I] λ6302, [O III] λ4363), suggesting the ionizing continuum is able to escape along channels to impact gas in the narrow line region.

3. The detections of N V without C IV or He II suggest elevated N V/C IV (> 1.4) and N V/He II (> 2.6) ratios, as have been seen in broad lines of nitrogen-loud quasars. We show that the line ratios can be reproduced by a combination of nitrogen-enhanced and turbulent gas, with a large ionization parameter and a shallow power law spectrum. The nitrogen enhancement may indicate the presence of top-heavy initial mass functions or tidal disruption events in the vicinity of the nucleus. The N V flux ratios may be further boosted by resonant scattering of Lyα photons which have been redshifted into the N V resonance by a fast outflow, as has been previously suggested for strong nitrogen emitting quasars (e.g., Hamann & Korista 1996; Wang et al. 2010). We suggest that if the densities of the NV-emitting gas are similar to that of the broad line region, it may help explain the weak He II emission and N IV] non-detection. The doublet ratios in both N V emitters are inconsistent with the expected intrinsic ratios, as may be expected

if the line emission is scattered through outflowing or inflowing gas. The resonant scattering of Lyα photons may further alter N V line ratios, while density-bounded gas may additionally play a role in driving the line ratios.

4. We explore the incidence of very high ionization emission (N V, He II, [Ne IV], [Ne V]) in a sample of 851 continuum-selected $z > 4$ galaxies and 18 $z > 4$ LRDs with moderate or high resolution NIRSpec observations covering the rest-frame UV. We find that $2.2^{+1.7}_{-1.0}$% of the $z > 4$ galaxy population has spectra with plausible detections of the very high ionization lines with EW > 10 Å. This fraction is comparable to that seen at lower redshifts in continuum-selected samples (Hainline et al. 2011), although a direct comparison is challenging given existing current EW limits. Most LRDs do not yet have spectra deep enough to constrain the full suite of narrow high ionization UV lines (N V, C IV, He II, [Ne IV], [Ne V]) to EWs of 10 Å, but the very limited samples suggest these lines are present in a subset of LRDs ($25.0^{+37.1}_{-20.8}$% for N V, $12.5^{+23.7}_{-10.4}$% for C IV). However, these results suggest that high ionization lines are weak in the majority of LRDs, potentially signally a softer ionizing spectrum or blanketing of the radiation field by dense neutral gas and dust.

5. The presence of narrow high ionization lines in LRDs with Balmer series absorption suggests that the extremely dense neutral hydrogen gas may not uniformly blanket the disk in all cases, enabling sightlines through which hard photons can be transmitted to the narrow line region. It is conceivable that the line-of-sight covering fraction of the dense neutral gas is non-unity. Alternatively, the ionizing radiation may largely escape through an excavated funnel along the polar axis, oriented perpendicular to the line-of-sight. The dense gas along the line-of-sight may significantly attenuate UV emission lines from the broad line region (if hydrogen is excited to the $n = 2$ level), potentially contributing to the weakness of the broad high ionization lines. Larger spectroscopic samples should reveal whether LRDs with high ionization lines differ in their properties from those that do not have high ionization features, allowing this picture to be tested in greater detail.

ACKNOWLEDGMENT

The authors would like to thank Linhua Jiang, Jianwei Lyu, Marta Volonteri, Feige Wang, and Huiyuan Wang for useful discussions. We also thank Stéphane Charlot and Jacopo Chevallard for providing access to the `BEAGLE` tool used for SED fitting analysis. MT acknowledges funding from the *JWST* Arizona/Steward Postdoc in Early galaxies and Reionization (JASPER) Scholar contract at the University of Arizona. DPS acknowledges support from the National Science Foundation through the grant AST-2109066. CAM acknowledges support by the European Union ERC grant RISES (101163035), Carlsberg Foundation (CF22-1322), and VILLUM FONDEN (37459). The Cosmic Dawn Center (DAWN) is funded by the Danish National Research Foundation under grant DNRF140. LW acknowledges support from the JWST/NIRCam contract to the University of Arizona, NAS5-02015, and support from the National Science Foundation Graduate Research Fellowship under Grant No. DGE-2137419.

This work is based on observations made with the NASA/ESA/CSA *James Webb Space Telescope*. The data were obtained from the Mikulski Archive for Space Telescopes at the Space Telescope Science Institute, which is operated by the Association of Universities for Research in Astronomy, Inc., under NASA contract NAS 5-03127 for *JWST*. These observations are associated with program GO 4287, and the following public-available programs GTO 1180, 1181, 1210, 1286, 1287, and GO 3215 (JADES; doi: 10.17909/8tdj-8n28), ERS 1324 (GLASS; doi: 10.17909/kw3c-n857), ERS 1345 and DDT 2750 (CEERS; doi: 10.17909/z7p0-8481), GO 1871, as well as GO 4233 (RUBIES). The authors acknowledge the JADES, GLASS, CEERS, and RUBIES teams led by Daniel Eisenstein & Nora Lüetzgendorf, K. Isaak, Tommaso Treu, Steven L. Finkelstein, Pablo Arrabal Haro, and Anna de Graaff & Gabriel Brammer for developing their observing programs. This research is also based in part on observations made with the NASA/ESA *Hubble Space Telescope* obtained from the Space Telescope Science Institute, which is operated by the Association of Universities for Research in Astronomy, Inc., under NASA contract NAS 5–26555. Part of the data products presented herein were retrieved from the Dawn *JWST* Archive (DJA). DJA is an initiative of the Cosmic Dawn Center, which is funded by the Danish National Research Foundation under grant DNRF140. This work is based in part upon High Performance Computing (HPC) resources supported by the University of Arizona TRIF, UITS, and Research, Innovation, and Impact (RII) and maintained by the UArizona Research Technologies department.

APPENDIX

A. GALAXIES WITH HIGH IONIZATION EMISSION LINES AT $Z > 4$

A.1. *GN-z11*

GN-z11 is a bright ($M_{UV} = -21.5$) galaxy at $z = 10.604$, with NIRSpec spectra (obtained from JADES GTO 1181) have been well studied previously (Bunker

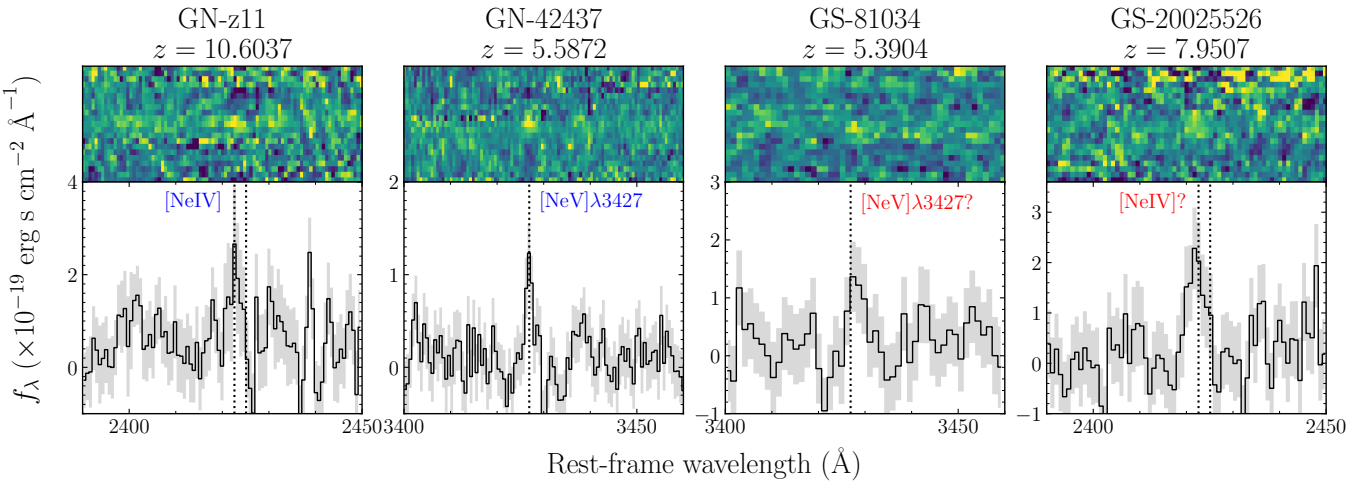

Figure 15. Plausible detections (S/N $\simeq 3-4$) of high ionization emission lines ([Ne V] and [Ne IV]) in the NIRSpec spectra of GN-z11, GN-42437, GS-81034, and GS-20025526.

et al. 2023). We derive a systemic redshift $z_{\rm sys} = 10.6037$ using the [Ne III] λ3869 and Hγ lines presented in the G395M spectrum, consistent with the value reported in Bunker et al. (2023). Using this redshift, we detect unresolved [Ne IV] $\lambda\lambda$2422, 2424 (S/N = 3) in the G235M spectrum. The [Ne IV] detection in GN-z11 was initially presented in Maiolino et al. (2024b), here we present our measurements for completeness. We measure a line flux $= 3.8 \pm 1.3 \times 10^{-19}$ erg s^{-1} cm^{-2}, consistent with the value ($3.14 \pm 0.65 \times 10^{-19}$ erg s^{-1} cm^{-2}) reported in Maiolino et al. (2024b). We derive a [Ne IV] EW $= 9.6 \pm 3.3$ Å.

A.2. *GN-42437*

GN-42437 is at $z_{\rm sys} = 5.5872$ with $M_{\rm UV} = -19.2$, with high-resolution ($R = 2700$) NIRSpec grating spectra obtained from program 1871 (Chisholm et al. 2024). We determine the systemic redshift from the [O III] doublet and Hα emission lines in the G395H spectrum, which is consistent with the redshift measured in Chisholm et al. (2024). Based on this redshift we find an emission line (S/N = 4) in the G235H spectrum with peak at 22573.2 Å, consistent with the line center of [Ne V] λ3427 (-6 ± 52 km s^{-1}). The [Ne V] detection of GN-42437 was initially reported in Chisholm et al. (2024). We measure a [Ne V] line flux $1.92 \pm 0.45 \times 10^{-19}$ erg s^{-1} cm^{-2} and EW $= 15 \pm 4$ Å, consistent with those reported in Chisholm et al. (2024) (line flux $= 2.35 \pm 0.34 \times 10^{-19}$ erg s^{-1} cm^{-2}, EW $= 11 \pm 2$ Å).

A.3. *GS-81034*

GS-81034 (R.A. = 53.088307, Decl. = -27.840416) is at $z_{\rm sys} = 5.3904$ with $M_{\rm UV} = -19.3$. Its medium-resolution ($R = 1000$) NIRSpec grating spectra were obtained from JADES program 1286. The systemic redshift of GS-81034 is determined from the Hβ, [O III], and Hα emission lines presented in the G395M spectrum. Using this redshift we identify a tentative (S/N = 3) emission feature in the G235M spectrum, with peak (21902.4 Å) consistent with the line center of [Ne V] λ3427 ($+42 \pm 107$ km s^{-1}). We measure a [Ne V] EW $= 15 \pm 5$ Å for GS-81034. We also examine whether the NIRSpec spectra reduced by other teams present this detection. We find that both the GS-81034 spectra reduced by the DJA and the JADES team show similar emission features at the line center of [Ne V] λ3427. We search for other high ionization emission lines in the spectra of GS-81034. We do not detect N V or C IV, He II emission, placing a 3σ upper limit of EW < 5 Å for each of these lines.

A.4. *GS-20025526*

GS-20025526 (R.A. = 53.099439, Decl. = -27.880489) is a bright galaxy ($M_{\rm UV} = -20.0$) at $z_{\rm sys} = 7.9507$, with $R = 1000$ NIRSpec spectra obtained from JADES GTO 1286. The systemic redshift is determined from the Hβ and [O III] emission lines in the G395M spectrum. Based on this redshift we detect an 3.5σ emission feature in the G235M spectrum with a peak at 21676.2 Å. This is consistent with the expected position of the unresolved [Ne IV] $\lambda\lambda$2422, 2424 doublet. We measure the [Ne IV] doublet EW $= 21 \pm 6$ Å. The similar [Ne IV] emission feature is also detected in the spectra reduced by the JADES team. In the spectra reduced by DJA, the emission feature is still presence but with a lower S/N ($\simeq 1.5$).] In the G140M spectrum of GS-20025526, we detect Lyα emission with EW $= 34\pm5$ Å, with peak velocity offset $= +426\pm96$ km s^{-1}. We do not detect N V emission, placing 3σ upper limit EW < 6 Å for each component of the doublet.

REFERENCES

Alarie, A., & Drissen, L. 2019, MNRAS, 489, 3042, doi: 10.1093/mnras/stz2279

Alexandroff, R., Strauss, M. A., Greene, J. E., et al. 2013, MNRAS, 435, 3306, doi: 10.1093/mnras/stt1500

Allen, M. G., Groves, B. A., Dopita, M. A., Sutherland, R. S., & Kewley, L. J. 2008, ApJS, 178, 20, doi: 10.1086/589652

Álvarez-Márquez, J., Crespo Gómez, A., Colina, L., et al. 2025, A&A, 695, A250, doi: 10.1051/0004-6361/202451731

Backhaus, B. E., Trump, J. R., Pirzkal, N., et al. 2024, ApJ, 962, 195, doi: 10.3847/1538-4357/ad1520

Baldwin, J. A., Hamann, F., Korista, K. T., et al. 2003, ApJ, 583, 649, doi: 10.1086/345449

Bekki, K., & Tsujimoto, T. 2023, MNRAS, 526, L26, doi: 10.1093/mnrasl/slad108

Bickel, W. 1969, JQSRT, 9, 1145, doi: 10.1016/0022-4073(69)90139-3

Böker, T., Beck, T. L., Birkmann, S. M., et al. 2023, PASP, 135, 038001, doi: 10.1088/1538-3873/acb846

Brinchmann, J. 2023, MNRAS, 525, 2087, doi: 10.1093/mnras/stad1704

Bunker, A. J., Saxena, A., Cameron, A. J., et al. 2023, A&A, 677, A88, doi: 10.1051/0004-6361/202346159

Bunker, A. J., Cameron, A. J., Curtis-Lake, E., et al. 2024, A&A, 690, A288, doi: 10.1051/0004-6361/202347094

Bushouse, H., Eisenhamer, J., Dencheva, N., et al. 2024, JWST Calibration Pipeline, 1.16.1, Zenodo, doi: 10.5281/zenodo.6984365

Caffau, E., Ludwig, H. G., Steffen, M., Freytag, B., & Bonifacio, P. 2011, SoPh, 268, 255, doi: 10.1007/s11207-010-9541-4

Cameron, A. J., Katz, H., Rey, M. P., & Saxena, A. 2023a, MNRAS, 523, 3516, doi: 10.1093/mnras/stad1579

Cameron, A. J., Katz, H., Witten, C., et al. 2024, MNRAS, 534, 523, doi: 10.1093/mnras/stae1547

Cameron, A. J., Saxena, A., Bunker, A. J., et al. 2023b, A&A, 677, A115, doi: 10.1051/0004-6361/202346107

Campbell, A., Terlevich, R., & Melnick, J. 1986, MNRAS, 223, 811, doi: 10.1093/mnras/223.4.811

Carniani, S., Hainline, K., D'Eugenio, F., et al. 2024, Nature, 633, 318, doi: 10.1038/s41586-024-07860-9

Castellano, M., Napolitano, L., Fontana, A., et al. 2024, ApJ, 972, 143, doi: 10.3847/1538-4357/ad5f88

Chang, S.-J., & Gronke, M. 2024, MNRAS, 532, 3526, doi: 10.1093/mnras/stae1664

Charlot, S., & Longhetti, M. 2001, MNRAS, 323, 887, doi: 10.1046/j.1365-8711.2001.04260.x

Chen, Z., Stark, D. P., Mason, C., et al. 2024, MNRAS, 528, 7052, doi: 10.1093/mnras/stae455

Chevallard, J., & Charlot, S. 2016, MNRAS, 462, 1415, doi: 10.1093/mnras/stw1756

Chisholm, J., Berg, D. A., Endsley, R., et al. 2024, MNRAS, 534, 2633, doi: 10.1093/mnras/stae2199

Coil, A. L., Aird, J., Reddy, N., et al. 2015, ApJ, 801, 35, doi: 10.1088/0004-637X/801/1/35

Cracco, V., Ciroi, S., Berton, M., et al. 2016, MNRAS, 462, 1256, doi: 10.1093/mnras/stw1689

Curti, M., Witstok, J., Jakobsen, P., et al. 2024, arXiv e-prints, arXiv:2407.02575, doi: 10.48550/arXiv.2407.02575

Davis, M., Guhathakurta, P., Konidaris, N. P., et al. 2007, ApJL, 660, L1, doi: 10.1086/517931

de Graaff, A., Brammer, G., Weibel, A., et al. 2024, arXiv e-prints, arXiv:2409.05948, doi: 10.48550/arXiv.2409.05948

de Graaff, A., Rix, H.-W., Naidu, R. P., et al. 2025, arXiv e-prints, arXiv:2503.16600, doi: 10.48550/arXiv.2503.16600

D'Eugenio, F., Maiolino, R., Carniani, S., et al. 2024, A&A, 689, A152, doi: 10.1051/0004-6361/202348636

D'Eugenio, F., Cameron, A. J., Scholtz, J., et al. 2025, ApJS, 277, 4, doi: 10.3847/1538-4365/ada148

Dong, X.-B., Ho, L. C., Wang, J.-G., et al. 2010, ApJL, 721, L143, doi: 10.1088/2041-8205/721/2/L143

Dors, O. L., Cardaci, M. V., Hägele, G. F., & Krabbe, Â. C. 2014, MNRAS, 443, 1291, doi: 10.1093/mnras/stu1218

Du, X., Shapley, A. E., Tang, M., et al. 2020, ApJ, 890, 65, doi: 10.3847/1538-4357/ab67b8

Eisenstein, D. J., Willott, C., Alberts, S., et al. 2023a, arXiv e-prints, arXiv:2306.02465, doi: 10.48550/arXiv.2306.02465

Eisenstein, D. J., Johnson, B. D., Robertson, B., et al. 2023b, arXiv e-prints, arXiv:2310.12340, doi: 10.48550/arXiv.2310.12340

Endsley, R., Stark, D. P., Whitler, L., et al. 2024, MNRAS, 533, 1111, doi: 10.1093/mnras/stae1857

Feltre, A., Charlot, S., & Gutkin, J. 2016, MNRAS, 456, 3354, doi: 10.1093/mnras/stv2794

Ferland, G. J., Porter, R. L., van Hoof, P. A. M., et al. 2013, RMxAA, 49, 137, doi: 10.48550/arXiv.1302.4485

Ferruit, P., Jakobsen, P., Giardino, G., et al. 2022, A&A, 661, A81, doi: 10.1051/0004-6361/202142673

Finkelstein, S. L., Bagley, M. B., Arrabal Haro, P., et al. 2025, ApJL, 983, L4, doi: 10.3847/2041-8213/adbbd3

Furtak, L. J., Labbé, I., Zitrin, A., et al. 2024, Nature, 628, 57, doi: 10.1038/s41586-024-07184-8

Gardner, J. P., Mather, J. C., Abbott, R., et al. 2023, PASP, 135, 068001, doi: 10.1088/1538-3873/acd1b5
Garnett, D. R. 1992, AJ, 103, 1330, doi: 10.1086/116146
Gehrels, N. 1986, ApJ, 303, 336, doi: 10.1086/164079
Grandi, S. A. 1980, ApJ, 238, 10, doi: 10.1086/157952
Greene, J. E., & Ho, L. C. 2005, ApJ, 630, 122, doi: 10.1086/431897
Greene, J. E., Labbe, I., Goulding, A. D., et al. 2024, ApJ, 964, 39, doi: 10.3847/1538-4357/ad1e5f
Groves, B. A., Dopita, M. A., & Sutherland, R. S. 2004, ApJS, 153, 9, doi: 10.1086/421113
Gutkin, J., Charlot, S., & Bruzual, G. 2016, MNRAS, 462, 1757, doi: 10.1093/mnras/stw1716
Hainich, R., Rühling, U., Todt, H., et al. 2014, A&A, 565, A27, doi: 10.1051/0004-6361/201322696
Hainline, K. N., Shapley, A. E., Greene, J. E., & Steidel, C. C. 2011, ApJ, 733, 31, doi: 10.1088/0004-637X/733/1/31
Hainline, K. N., Maiolino, R., Juodžbalis, I., et al. 2025, ApJ, 979, 138, doi: 10.3847/1538-4357/ad9920
Hamann, F., & Ferland, G. 1992, ApJL, 391, L53, doi: 10.1086/186397
—. 1993, ApJ, 418, 11, doi: 10.1086/173366
Hamann, F., & Korista, K. T. 1996, ApJ, 464, 158, doi: 10.1086/177307
Harikane, Y., Zhang, Y., Nakajima, K., et al. 2023, ApJ, 959, 39, doi: 10.3847/1538-4357/ad029e
Heintz, K. E., Watson, D., Brammer, G., et al. 2024, Science, 384, 890, doi: 10.1126/science.adj0343
Hirschmann, M., Charlot, S., Feltre, A., et al. 2019, MNRAS, 487, 333, doi: 10.1093/mnras/stz1256
Hsiao, T. Y.-Y., Abdurro'uf, Coe, D., et al. 2024, ApJ, 973, 8, doi: 10.3847/1538-4357/ad5da8
Hu, W., Papovich, C., Dickinson, M., et al. 2024, ApJ, 971, 21, doi: 10.3847/1538-4357/ad5015
Hutchison, T. A., Papovich, C., Finkelstein, S. L., et al. 2019, ApJ, 879, 70, doi: 10.3847/1538-4357/ab22a2
Inayoshi, K., & Maiolino, R. 2025, ApJL, 980, L27, doi: 10.3847/2041-8213/adaebd
Isobe, Y., Ouchi, M., Nakajima, K., et al. 2023, ApJ, 956, 139, doi: 10.3847/1538-4357/acf376
Isobe, Y., Maiolino, R., D'Eugenio, F., et al. 2025, arXiv e-prints, arXiv:2502.12091, doi: 10.48550/arXiv.2502.12091
Izotov, Y. I., Thuan, T. X., & Privon, G. 2012, MNRAS, 427, 1229, doi: 10.1111/j.1365-2966.2012.22051.x
Jakobsen, P., Ferruit, P., Alves de Oliveira, C., et al. 2022, A&A, 661, A80, doi: 10.1051/0004-6361/202142663
Ji, X., Übler, H., Maiolino, R., et al. 2024, MNRAS, 535, 881, doi: 10.1093/mnras/stae2375
Ji, X., Maiolino, R., Übler, H., et al. 2025, arXiv e-prints, arXiv:2501.13082, doi: 10.48550/arXiv.2501.13082
Jiang, L., Fan, X., & Vestergaard, M. 2008, ApJ, 679, 962, doi: 10.1086/587868
Jiang, Y.-F., Stone, J. M., & Davis, S. W. 2019, ApJ, 880, 67, doi: 10.3847/1538-4357/ab29ff
Juodžbalis, I., Ji, X., Maiolino, R., et al. 2024, MNRAS, 535, 853, doi: 10.1093/mnras/stae2367
Juodžbalis, I., Maiolino, R., Baker, W. M., et al. 2025, arXiv e-prints, arXiv:2504.03551. https://arxiv.org/abs/2504.03551
Kewley, L. J., Dopita, M. A., Sutherland, R. S., Heisler, C. A., & Trevena, J. 2001, ApJ, 556, 121, doi: 10.1086/321545
Kobayashi, C., & Ferrara, A. 2024, ApJL, 962, L6, doi: 10.3847/2041-8213/ad1de1
Kocevski, D. D., Onoue, M., Inayoshi, K., et al. 2023, ApJL, 954, L4, doi: 10.3847/2041-8213/ace5a0
Kocevski, D. D., Finkelstein, S. L., Barro, G., et al. 2024, arXiv e-prints, arXiv:2404.03576, doi: 10.48550/arXiv.2404.03576
Kochanek, C. S. 2016, MNRAS, 458, 127, doi: 10.1093/mnras/stw267
Kokorev, V., Fujimoto, S., Labbe, I., et al. 2023, ApJL, 957, L7, doi: 10.3847/2041-8213/ad037a
Kokorev, V., Caputi, K. I., Greene, J. E., et al. 2024, ApJ, 968, 38, doi: 10.3847/1538-4357/ad4265
Kraemer, S. B., & Crenshaw, D. M. 2000, ApJ, 544, 763, doi: 10.1086/317246
Krolik, J. H., & Voit, G. M. 1998, ApJL, 497, L5, doi: 10.1086/311274
Kumari, N., Smit, R., Witstok, J., et al. 2024, arXiv e-prints, arXiv:2406.11997, doi: 10.48550/arXiv.2406.11997
Kuraszkiewicz, J. K., Green, P. J., Crenshaw, D. M., et al. 2004, ApJS, 150, 165, doi: 10.1086/379809
Kwan, J., & Krolik, J. H. 1981, ApJ, 250, 478, doi: 10.1086/159395
Labbé, I., van Dokkum, P., Nelson, E., et al. 2023, Nature, 616, 266, doi: 10.1038/s41586-023-05786-2
Labbe, I., Greene, J. E., Matthee, J., et al. 2024, arXiv e-prints, arXiv:2412.04557, doi: 10.48550/arXiv.2412.04557
Labbe, I., Greene, J. E., Bezanson, R., et al. 2025, ApJ, 978, 92, doi: 10.3847/1538-4357/ad3551
Lambrides, E., Garofali, K., Larson, R., et al. 2024, arXiv e-prints, arXiv:2409.13047, doi: 10.48550/arXiv.2409.13047
Laporte, N., Nakajima, K., Ellis, R. S., et al. 2017, ApJ, 851, 40, doi: 10.3847/1538-4357/aa96a8

Le Fèvre, O., Lemaux, B. C., Nakajima, K., et al. 2019, A&A, 625, A51, doi: 10.1051/0004-6361/201732197
Lin, X., Wang, F., Fan, X., et al. 2024, ApJ, 974, 147, doi: 10.3847/1538-4357/ad6565
Luridiana, V., Morisset, C., & Shaw, R. A. 2015, A&A, 573, A42, doi: 10.1051/0004-6361/201323152
Lusso, E., Worseck, G., Hennawi, J. F., et al. 2015, MNRAS, 449, 4204, doi: 10.1093/mnras/stv516
Madau, P. 1988, ApJ, 327, 116, doi: 10.1086/166175
—. 2025, arXiv e-prints, arXiv:2501.09854, doi: 10.48550/arXiv.2501.09854
Madau, P., & Haardt, F. 2024, ApJL, 976, L24, doi: 10.3847/2041-8213/ad90e1
Mainali, R., Kollmeier, J. A., Stark, D. P., et al. 2017, ApJL, 836, L14, doi: 10.3847/2041-8213/836/1/L14
Mainali, R., Stark, D. P., Tang, M., et al. 2020, MNRAS, 494, 719, doi: 10.1093/mnras/staa751
Maiolino, R., Scholtz, J., Curtis-Lake, E., et al. 2024a, A&A, 691, A145, doi: 10.1051/0004-6361/202347640
Maiolino, R., Scholtz, J., Witstok, J., et al. 2024b, Nature, 627, 59, doi: 10.1038/s41586-024-07052-5
Martínez-Aldama, M. L., Dultzin, D., Marziani, P., et al. 2015, ApJS, 217, 3, doi: 10.1088/0067-0049/217/1/3
Masters, D., McCarthy, P., Siana, B., et al. 2014, ApJ, 785, 153, doi: 10.1088/0004-637X/785/2/153
Matsuoka, K., Nagao, T., Marconi, A., Maiolino, R., & Taniguchi, Y. 2011, A&A, 527, A100, doi: 10.1051/0004-6361/201015584
Matthee, J., Naidu, R. P., Brammer, G., et al. 2024, ApJ, 963, 129, doi: 10.3847/1538-4357/ad2345
Mazzolari, G., Scholtz, J., Maiolino, R., et al. 2024a, arXiv e-prints, arXiv:2408.15615, doi: 10.48550/arXiv.2408.15615
Mazzolari, G., Übler, H., Maiolino, R., et al. 2024b, A&A, 691, A345, doi: 10.1051/0004-6361/202450407
McClymont, W., Tacchella, S., D'Eugenio, F., et al. 2024, arXiv e-prints, arXiv:2405.15859, doi: 10.48550/arXiv.2405.15859
Mignoli, M., Feltre, A., Bongiorno, A., et al. 2019, A&A, 626, A9, doi: 10.1051/0004-6361/201935062
Nagao, T., Maiolino, R., & Marconi, A. 2006a, A&A, 447, 863, doi: 10.1051/0004-6361:20054127
Nagao, T., Marconi, A., & Maiolino, R. 2006b, A&A, 447, 157, doi: 10.1051/0004-6361:20054024
Naidu, R. P., Matthee, J., Katz, H., et al. 2025, arXiv e-prints, arXiv:2503.16596, doi: 10.48550/arXiv.2503.16596
Nakajima, K., Ouchi, M., Isobe, Y., et al. 2023, ApJS, 269, 33, doi: 10.3847/1538-4365/acd556
Nakajima, K., Schaerer, D., Le Fèvre, O., et al. 2018, A&A, 612, A94, doi: 10.1051/0004-6361/201731935
Napolitano, L., Castellano, M., Pentericci, L., et al. 2024, arXiv e-prints, arXiv:2410.18763, doi: 10.48550/arXiv.2410.18763
—. 2025, A&A, 693, A50, doi: 10.1051/0004-6361/202452090
Netzer, H., Elitzur, M., & Ferland, G. J. 1985, ApJ, 299, 752, doi: 10.1086/163741
Oke, J. B., & Gunn, J. E. 1983, ApJ, 266, 713, doi: 10.1086/160817
Osterbrock, D. E., & Ferland, G. J. 2006, Astrophysics of gaseous nebulae and active galactic nuclei
Pacucci, F., & Narayan, R. 2024, ApJ, 976, 96, doi: 10.3847/1538-4357/ad84f7
Pognan, Q., Trakhtenbrot, B., Sbarrato, T., Schawinski, K., & Bertemes, C. 2020, MNRAS, 492, 4058, doi: 10.1093/mnras/staa078
Rieke, M. J., Kelly, D., & Horner, S. 2005, in Society of Photo-Optical Instrumentation Engineers (SPIE) Conference Series, Vol. 5904, Cryogenic Optical Systems and Instruments XI, ed. J. B. Heaney & L. G. Burriesci, 1–8, doi: 10.1117/12.615554
Rieke, M. J., Kelly, D. M., Misselt, K., et al. 2023, PASP, 135, 028001, doi: 10.1088/1538-3873/acac53
Riffel, R., Rodríguez-Ardila, A., & Pastoriza, M. G. 2006, A&A, 457, 61, doi: 10.1051/0004-6361:20065291
Rigby, J., Perrin, M., McElwain, M., et al. 2023, PASP, 135, 048001, doi: 10.1088/1538-3873/acb293
Roberts-Borsani, G., Treu, T., Shapley, A., et al. 2024, ApJ, 976, 193, doi: 10.3847/1538-4357/ad85d3
Rodríguez-Ardila, A., Viegas, S. M., Pastoriza, M. G., Prato, L., & Donzelli, C. J. 2002, ApJ, 572, 94, doi: 10.1086/340192
Rose, M., Elvis, M., & Tadhunter, C. N. 2015, MNRAS, 448, 2900, doi: 10.1093/mnras/stv113
Sanders, R. L., Shapley, A. E., Topping, M. W., Reddy, N. A., & Brammer, G. B. 2023, ApJ, 955, 54, doi: 10.3847/1538-4357/acedad
—. 2024, ApJ, 962, 24, doi: 10.3847/1538-4357/ad15fc
Sanders, R. L., Shapley, A. E., Reddy, N. A., et al. 2020, MNRAS, 491, 1427, doi: 10.1093/mnras/stz3032
Scarlata, C., Hayes, M., Panagia, N., et al. 2024, arXiv e-prints, arXiv:2404.09015, doi: 10.48550/arXiv.2404.09015
Scholtz, J., Maiolino, R., D'Eugenio, F., et al. 2023, arXiv e-prints, arXiv:2311.18731, doi: 10.48550/arXiv.2311.18731
Senchyna, P., Plat, A., Stark, D. P., et al. 2024, ApJ, 966, 92, doi: 10.3847/1538-4357/ad235e

Shapley, A. E., Reddy, N. A., Sanders, R. L., Topping, M. W., & Brammer, G. B. 2023, ApJL, 950, L1, doi: 10.3847/2041-8213/acd939

Shapley, A. E., Steidel, C. C., Pettini, M., & Adelberger, K. L. 2003, ApJ, 588, 65, doi: 10.1086/373922

Shapley, A. E., Sanders, R. L., Topping, M. W., et al. 2025, ApJ, 980, 242, doi: 10.3847/1538-4357/adad68

Sikora, M. 1981, MNRAS, 196, 257, doi: 10.1093/mnras/196.2.257

Silcock, M. S., Curtis-Lake, E., Smith, D. J. B., et al. 2024, arXiv e-prints, arXiv:2410.18193, doi: 10.48550/arXiv.2410.18193

Stark, D. P., Richard, J., Siana, B., et al. 2014, MNRAS, 445, 3200, doi: 10.1093/mnras/stu1618

Stark, D. P., Richard, J., Charlot, S., et al. 2015a, MNRAS, 450, 1846, doi: 10.1093/mnras/stv688

Stark, D. P., Walth, G., Charlot, S., et al. 2015b, MNRAS, 454, 1393, doi: 10.1093/mnras/stv1907

Stark, D. P., Ellis, R. S., Charlot, S., et al. 2017, MNRAS, 464, 469, doi: 10.1093/mnras/stw2233

Surdej, J., & Hutsemekers, D. 1987, A&A, 177, 42

Tang, M., Stark, D. P., Chevallard, J., & Charlot, S. 2019, MNRAS, 489, 2572, doi: 10.1093/mnras/stz2236

Tang, M., Stark, D. P., Chevallard, J., et al. 2021, MNRAS, 501, 3238, doi: 10.1093/mnras/staa3454

Tang, M., Stark, D. P., Topping, M. W., Mason, C., & Ellis, R. S. 2024, ApJ, 975, 208, doi: 10.3847/1538-4357/ad7eb7

Tang, M., Stark, D. P., Chen, Z., et al. 2023, MNRAS, 526, 1657, doi: 10.1093/mnras/stad2763

Taylor, A. J., Finkelstein, S. L., Kocevski, D. D., et al. 2024, arXiv e-prints, arXiv:2409.06772, doi: 10.48550/arXiv.2409.06772

Topping, M. W., Shapley, A. E., Stark, D. P., et al. 2021, ApJL, 917, L36, doi: 10.3847/2041-8213/ac1a79

Topping, M. W., Stark, D. P., Senchyna, P., et al. 2024a, MNRAS, 529, 3301, doi: 10.1093/mnras/stae682

Topping, M. W., Stark, D. P., Endsley, R., et al. 2024b, MNRAS, 529, 4087, doi: 10.1093/mnras/stae800

Topping, M. W., Stark, D. P., Senchyna, P., et al. 2025a, ApJ, 980, 225, doi: 10.3847/1538-4357/ada95c

Topping, M. W., Sanders, R. L., Shapley, A. E., et al. 2025b, arXiv e-prints, arXiv:2502.08712. https://arxiv.org/abs/2502.08712

Treiber, H., Greene, J., Weaver, J. R., et al. 2024, arXiv e-prints, arXiv:2409.12232, doi: 10.48550/arXiv.2409.12232

Treu, T., Roberts-Borsani, G., Bradac, M., et al. 2022, ApJ, 935, 110, doi: 10.3847/1538-4357/ac8158

Tripodi, R., Martis, N., Markov, V., et al. 2024, arXiv e-prints, arXiv:2412.04983, doi: 10.48550/arXiv.2412.04983

Trump, J. R., Arrabal Haro, P., Simons, R. C., et al. 2023, ApJ, 945, 35, doi: 10.3847/1538-4357/acba8a

Turnshek, D. A., Foltz, C. B., Grillmair, C. J., & Weymann, R. J. 1988, ApJ, 325, 651, doi: 10.1086/166036

Übler, H., Maiolino, R., Curtis-Lake, E., et al. 2023, A&A, 677, A145, doi: 10.1051/0004-6361/202346137

Übler, H., Maiolino, R., Pérez-González, P. G., et al. 2024, MNRAS, 531, 355, doi: 10.1093/mnras/stae943

Valentino, F., Brammer, G., Gould, K. M. L., et al. 2023, ApJ, 947, 20, doi: 10.3847/1538-4357/acbefa

Vidal-García, A., Plat, A., Curtis-Lake, E., et al. 2024, MNRAS, 527, 7217, doi: 10.1093/mnras/stad3252

Vink, J. S. 2022, ARA&A, 60, 203, doi: 10.1146/annurev-astro-052920-094949

Walborn, N. R., & Panek, R. J. 1984, ApJL, 280, L27, doi: 10.1086/184262

Wang, B., de Graaff, A., Davies, R. L., et al. 2024a, arXiv e-prints, arXiv:2403.02304, doi: 10.48550/arXiv.2403.02304

Wang, B., Leja, J., de Graaff, A., et al. 2024b, ApJL, 969, L13, doi: 10.3847/2041-8213/ad55f7

Wang, H., Wang, T., Yuan, W., et al. 2010, ApJ, 710, 78, doi: 10.1088/0004-637X/710/1/78

Wang, J.-M., Qiu, J., Du, P., & Ho, L. C. 2014, ApJ, 797, 65, doi: 10.1088/0004-637X/797/1/65

Weymann, R. J., Morris, S. L., Foltz, C. B., & Hewett, P. C. 1991, ApJ, 373, 23, doi: 10.1086/170020